Ephrin-B1 is a novel specific component of the lateral membrane of the cardiomyocyte and is essential for the stability of cardiac tissue architecture cohesion

Gaël Genet[*], Céline Guilbeau-Frugier[*], Benjamin Honton, Etienne Dague, Michael D. Schneider, Christelle Coatrieux, Denis Calise, Christelle Cardin, Cécile Nieto, Bruno Payré, Caroline Dubroca, Pauline Marck, Christophe Heymes, Alexandre Dubrac, Dina Arvanitis, Fabien Despas, Marie-Françoise Altié, Marie-Hélène Seguelas, Marie-Bernadette Delisle, Alice Davy, Jean-Michel Sénard, Atul Pathak, Céline Galés.

Short title: Role of ephrin-B1 in cardiomyocyte architecture

Authors' affiliations:
Institut des Maladies Métaboliques et Cardiovasculaires, Institut National de la Santé et de la Recherche Médicale UMR 1048, (G.G, B.H., C.C., F.D., M.F.A., M.H.S., J.M.S., A.P., C.G., A.D., D.C.), Department of Histopathology (C.G.F, M.B.D) and of Clinical Pharmacology (F.D., J.M.S., A.P.), Toulouse University Hospital , CNRS; LAAS, ITAV-UMS3039 (E.D.), Centre de Microscopie Électronique Appliquée à la Biologie, Rangueil Medical faculty (C.N., BP), Development biology center, CNRS, UMR 5547 (D.A., A.D.), Paul Sabatier University Toulouse III, France. National Heart and Lung Institute, Imperial College London, London, UK (M.D.S.).

Authors contributions:
[*] G.G. and C.G.F. contributed equally to this work.

Corresponding author: Dr Galés Céline.
Adress: Inserm U1048
Institut des Maladies Métaboliques et Cardiovasculaires - I2MC
1, avenue Jean-Poulhès - BP84225
31432 Toulouse cedex 4
France
Phone: 33-5-61-32-29-21
Fax: 33-5 62 17 25 54
Email: celine.gales@inserm.fr

The authors declared that no conflict of interest exists.

Abstract

***Rationale*:** Cardiac tissue cohesion relying on highly ordered cardiomyocytes (CMs) interactions, is critical since most cardiomyopathies are associated with tissue remodelling and architecture alterations.
***Objective*:** Eph/ephrin system constitutes a ubiquitous system coordinating cellular communications which recently emerged as a major regulator in adult organs. We examined if eph/ephrin could participate in cardiac tissue cytoorganization.
Methods and Results: We reported for the first time the expression of cardiac ephrin-B1 in both endothelial cells and CMs. In CMs, ephrin-B1 displayed specific localization at the lateral membrane. Ephrin-B1 knock-out (KO) mice progressively developed cardiac tissue disorganization with loss of adult CM rod-shape and sarcomeric and intercalated disk structural disorganization confirmed in CM-specific ephrin-B1 KO mice (cKO). CMs lateral membrane exhibited abnormal structure and increased stiffness as shown by electronic and atomic force microscopy. In wild-type CMs, ephrin-B1 interacted with claudin-5/ZO-1 complex at the lateral membrane while the complex disappeared in KO/cKO mice. Ephrin-B1 deficiency resulted in decreased mRNA expression of CM basement membrane components and disorganized fibrillar collagen matrix, independently of classical integrin/dystroglycan system. KO/cKO mice exhibited increased left ventricle diameter and delayed atrioventricular conduction. Under pressure overload stress, KO mice were prone to death and exhibited striking tissue disorganization correlating with heart failure. Finally, failing CMs displayed downregulated ephrin-B1/claudin-5 gene expression linearly related to the ejection fraction.
Conclusions: Ephrin-B1 is necessary for cardiac tissue architecture cohesion by stabilizing the adult CM morphology through regulation of its lateral membrane. Since decreased ephrin-B1 associated with molecular/functional cardiac defects, it could represent a new actor in the transition toward heart failure.

Key Words: cardiomyocyte – extracellular matrix – lateral membrane – cardiac tissue architecture – heart failure

Non standard Abbreviations and Acronyms

AFM Atomic Force Microscopy
CM Cardiomyocyte
EC Endothelial Cell
ECM Extracellular matrix
HF Heart failure
I-B4 Isolectine-B4
ID Intercalated Disk
KO Knock-out
WGA Wheat Germ Agglutinin
WT Wild-Type

Introduction

The heart constitutes a particular compact organ relying on strong tissue architecture cohesion and tight cellular interactions that ensure both mechanical and electrochemical coupling. Thus, most cardiopathies are associated with cardiac tissue remodelling and with alterations in architecture involved in disease progression toward heart failure (HF). Despite considerable advances in the field and development of effective drugs, HF still remains a prevalent condition associated with high morbidity and mortality rates. This could be in part explained by still imperfect knowledge of molecular basis at the origin of HF. In fact, to date, most research has focused on cardiomyocyte (CM) contractile dysfunction but has essentially ignored the importance of modifications in CM interactions with their environment in the cardiac tissue. Thus, a thorough analysis of CM interactions involved in the stability of cardiac tissue architecture may help in the identification of new potential therapeutic targets for prevention and treatment of cardiac remodelling leading to heart failure.

Functional adult CMs are organized within the tissue through both cell-cell interactions involving end-to-end contacts via the intercalated disk (ID) and cell-matrix interactions through receptors localized along the sarcolemma. Together, these structures control connections of contractile myofilaments to the plasma membrane of the CM and have garnered attention due to their involvement in cardiac diseases [1, 2]. Despite numerous junctions present at the ID have been well characterized [3], little is known regarding the molecular nature of lateral membrane components. To date, only integrin and sarcoglycan systems specifically connecting contractile apparatus of the CM to the extracellular matrix (ECM) have been described [4, 5].

Eph receptor tyrosine kinases and their membrane-bound ligands ephrins form an essential intercellular communication system associated with cytoskeleton regulations [6]. In the last few years, the role of Eph/ephrin system has been extensively investigated mainly in developing tissues, including the central nervous and vascular system. Eph/ephrins have been implicated in various processes including neuronal network formation, guidance of migrating cells, axonal pathfinding but also in the regulation of angiogenesis [7, 8]. More recently, Eph/ephrins have been shown to be major actors in the pathophysiology of cancer [9]. So far, little is known regarding their putative roles in adult tissue but they have been reported to participate in modulation of bone remodelling [10] and insulin secretion [11]. Finally, their role in the control of cell-cell interactions has been underlined in kidney [12] and crystalline lens [13] emphasizing the importance of ephrin system in maintaining tissue architecture.

A role for EphA3 receptor has been identified in heart development and morphogenesis at the embryonic stage [14]. However, the Eph/ephrin system has never been explored in adult cardiac tissue. In fact, mutations in the ephrin-B1 gene in humans have been associated with Cranio Frontonasal Syndrome which is characterized by craniofacial dysmorphies with some of the mutations associated also with cardiomyopathy [15]. Moreover, several studies have reported specific ephrin-B1 regulation of cellular junctions such as gap junctions [16], tight junctions [17] and also ECM receptors [18, 19]. All of these junctions are important regulators for cell and tissue cohesion and are altered in different models of cardiomyopathy. Thus, we decided to explore the potential cardiac role of ephrin-B1.

In the present study, using an ephrin-B1 knockout (KO) mouse model (*efnb1*$^{-/-}$), we identified ephrin-B1 as a new structural protein specific for the lateral membrane of the CM involved in adult cardiac tissue architecture stabilization. Using a wide array of approaches from light and electron microscopy, nanomechanical and biochemical measurements to *in vivo* functional assays, we show that the lack of ephrin-B1 leads to cardiac tissue alterations that may predispose to pathological responses under cardiac stress.

Methods

An expanded methods section is available in the Online Data Supplement.

Statistical analysis. All data represent the mean ± S.E.M. of 3 to 10 independent experiments as indicated. Statistical significance of the data was assessed using unpaired 2-tailed Student's *t* test (**P* < 0.05, ***P* < 0.01, ***P < 0.001, ns, non significant). In some cases, Chi square test was used instead (Kaplan-Meier curves).

Results

Ephrin-B1 is largely expressed in cardiac muscle and is specific of the endothelial cell and the lateral membrane of the mature adult cardiomyocyte

We first assessed the expression of ephrin-B1 in adult heart from wild-type (WT) mice. Western-blot analysis revealed abundant and specific expression of ephrin-B1 in whole cardiac tissue extracts (Figure 1A). Fluorescence imaging of heart cryosections revealed that ephrin-B1 was expressed in all heart compartments (left and right ventricles, septum) (not shown). Cell membrane Wheat Germ Agglutinin (WGA) co-staining showed that the protein was specifically expressed at the lateral membrane of cardiomyocytes (CMs) with no expression in the intercalated disk (ID) (Figure 1 B-C).. Similar pattern of ephrin-B1 expression was obtained in CMs from adult rat cardiac tissue (Online Figure I, A). Beside CM staining, ephrin-B1 was also detected in endothelial cells (ECs) from both micro- and macrovasculature as demonstrated by co-localization with isolectin-B4 (I-B4), a specific EC marker (Figure 1 B-C). Both CMs and ECs staining were completely lost in KO mice demonstrating the specificity for ephrin-B1 cardiac expression and localization (Figure 1B). Compartmentalizations of ephrin-B1 at both lateral membrane of CMs and ECs were further confirmed by immunogold electron microscopy (Figure 1D). Interestingly, ephrin-B1 localization in the CM was regulated during postnatal myocardial maturation period (3 weeks). Indeed, ephrin-B1 was totally absent from the lateral membrane of the CM the first postnatal days when it was only expressed in the nucleus (Online Figure I, A), while its expression at the lateral membrane correlated with the final adult CM maturation step, most likely indicating a specific role of this protein after birth in the lateral membrane of the mature CM. By opposition, ephrin-B1 expression/localization in adult ECs was already detected in ECs immediately after birth (Online Figure IB).

Ephrin-B1 knockdown disrupts cardiac tissue architecture cohesion and cardiomyocyte morphology

To understand the role of ephrin-B1 in the mature CM, we analyzed the cardiac phenotype of the general ephrin-B1 KO mice which were previously described [20]. We first undertook a histological analysis using H&E staining of cardiac tissue from WT and KO mice at different development stages (3 weeks and 2 months). Three weeks after birth, there was no evidence for cardiac tissue modification in KO mice compared with WT (Figure 2A, upper). However, at 2 months of age, in contrast to WT hearts characterized by a tight and strong cohesion between CMs, disorganization of CMs with a "wavy" aspect could be visualized randomly in all heart compartments (septum, right and left ventricle) from KO mice (Figure 2A, middle) with some CMs exhibiting whorled appearance (Figure 2A, lower). These changes were detected in all KO mice, but present focal distribution within the tissue. Thus, ephrin-B1 KO mice developed progressive alteration of the cardiac tissue architecture which correlated with the timing of ephrin-B1 lateral membrane expression in the mature adult CM from WT animals. Morphometric analysis of cell membranes by WGA-staining further confirmed modification of CMs morphology that lost their hallmark rod-shape (Figure 2B). Quantification studies demonstrated significant decrease in cross-sectional area of CMs from KO mice in fixated cardiac tissue (Figure 2C) with no difference in cell density (WT: 10.6 ±0.7 CMs per mm^2; KO: 11.3 ± 1.1 CMs cells per mm^2). In agreement with tissue observations, isolated adult KO CMs displayed a significant reduced short axis while increasing their long axis compared with WT (Figure 2D). Even though KO mice displayed CMs morphology abnormalities, this was not correlated with development of cardiac fibrosis (Online Figure II, A). Aberrant cell differentiation during heart development could not account for morphological CM changes in KO mice, since all 3 weeks-old mice exhibited mature rod-shape CMs and tissue alterations were evident only 2 months after birth. ~~Moreover, KO animals did not exhibit cardiac development abnormalities precluding a major role for ephrin-B1 in cardiogenesis.~~ It is noteworthy that despite broad expression of ephrin-B1 in the cardiac capillary network, 2-months old KO mice showed no changes in capillary density as quantified by Isolectin-B4 ECs-staining (Online Figure II, B) nor evidence for myocardial necrosis or inflammation as visualized on H&E staining, thus demonstrating integrity and functionality of the cardiac vasculature. Altogether, these results supported a role for ephrin-B1 in the maintenance of adult cardiac tissue architecture essentially by controlling CMs morphology.

Ephrin-B1 regulates the cardiomyocyte lateral membrane structure and nanomechanical properties through stabilization of claudin-5

Given the specific expression of ephrin-B1 at the lateral membrane of the CM, we questioned whether disturbance of the lateral membrane accounted for the abnormal CM morphology in KO mice. Electron microscopy revealed significant structural alterations of the lateral junction characterized by an abnormal non linear appearance compared with WT mice (Figure 3A). To rule out contribution of other cardiac cell types in the CM phenotype, we generated a cardiomyocyte-specific ephrin-B1 KO mice (cKO) (Online Figure III). In cKO mice, we confirmed lateral membrane disorganization of the CM (Online Figure IV, A). In correlation with the alteration of the CM lateral membrane structure, atomic force microscopy (AFM) study revealed a significant 3 fold increase of Young Modulus (Elasticty) in CMs from KO mice ranging from 35.5 ± 6.4 kPa to 62.4 ± 13.1 kPa compared with 12.5 ± 1.3 kPa to 21.3 ±3.6 kPa in WT mice (Figure 3B, lower panel), thus indicating that the lack of ephrin-B1 in the CM increased the stiffness of the lateral membrane. It must be noticed that the repartition of Young Modulus was very homogeneous throughout the lateral membrane of WT CMs, while it showed high heterogeneity in KO CMs as represented by the larger distribution of young modulus frequency (Figure 3B, right panels), most probably reflecting different levels of morphology modifications at the lateral membrane surface.

To understand the molecular basis accounting for this phenotype and given the interaction of the lateral membrane of the CM with the extracellular matrix, CM-matrix interactions predominantly regulated by integrin- and dystroglycan-based complexes were first analyzed. We found that localization (Online Figure V, A) and expression (Online Figure V, B) of both β1-integrin and β-sarcoglycan/α-dystroglycan (glycosylation) complex along the plasma membrane were unchanged in hearts from KO mice compared to WT as shown by immunofluorescence and immunoblot staining respectively, thus demonstrating regular and functional CM-matrix junction complexes in the absence of ephrin-B1. We looked then at the tight junction transmembrane protein claudin-5, a specific endothelial cell tight junction component, which was previously localized at the lateral membrane of the CM and whose downregulation correlated with similar modification of lateral membrane structure in mice models of cardiomyopathy to that observed in ephrin-B1 KO mice [21]. We confirmed the presence of claudin-5 in the microcirculation and along the lateral membrane of CMs in control hearts (Figure 3C; Online Figure IV, B) and did not detect any labelling in the ID. Specific expression of claudin-5 at the lateral membrane of the CM was more readily detectable in rat heart (Online Figure V, C). By contrast, claudin-5 was completely absent from the lateral membrane in both general and conditional ephrin-B1 KO mice (Figure 3C and Online Figure IV, B) and showed specific downregulation as revealed by the significant decrease in protein (Figure 3D), and gene expression level (Figure 3E), thus suggesting specific regulation of claudin-5 by ephrin-B1. Similarly, the intracellular scaffolding claudin-associated-protein ZO-1, which was detected at both lateral membrane and ID in CMs from control hearts (Figure 3C, left panel and Online Figure IV, C), disappeared from the lateral junction in KO and cKO mice (Figure 3C and Online Figure IV, C). However, ZO-1 further accumulated in the ID as evidence by the significant increase in ZO-1 fluorescent staining (Figure 3C, WT: 112.0 ± 6.2 fluorescence/pixel², KO: 138.3 ± 8.2 fluorescence/pixel², means ± SEM, $P<0.05$). Relocalization of ZO-1 was further supported by the lack of modification of ZO-1 protein (Figure 3D) and gene expression (Figure 3E). Altogether, these results supported a role for ephrin-B1 in the stabilization of claudin-5/ZO-1 junctional complex at the lateral membrane of the CM. The regulation of claudin-5 by ephrin-B1 at the lateral membrane most likely relates to a direct mechanism since both claudin-5 and its ZO-1 partner were found associated with ephrin-B1 in isolated CMs as shown by co-immunoprecipitation (Figure 3F) and claudin-5 could directly interact with ephrin-B1 in BRET experiments (Figure 3G). Specific destabilization of claudin-5/ZO-1 complex in ephrin-B1 KO mice most likely preceded and initiated the lateral membrane disorganization of the CM. Indeed, lack of claudin-5 at the lateral membrane was evident in all CMs from 2 month-old KO mice while modification of their lateral membrane structure was only focal at same age. It follows that ephrin-B1 may regulate the morphology of the CM by controlling lateral membrane structure through a mechanism involving the specific adhesion protein claudin-5.

Ephrin-B1 knockdown impairs basement membrane of the cardiomyocyte and fibrillar collagens organization

Because CMs are anchored to the extracellular matrix (ECM) through their lateral membrane and ephrin-B1 KO mice exhibited structural alteration of the lateral membrane, we examined the morphology of cardiac ECM from KO and WT mice by electron microscopy. In contrast to the well-organized pattern in WT, the basement membrane and the fibrillar collagen bundles were highly disorganized in the KO mice (Figure 4A) as well in cKO mice (Online Figure IV, D), most likely indicating destabilization of the overall ECM structure. Interstitial space separating two adjacent CMs was irregular in all ephrin-B1 KO/cKO mice (Figure 4A, Online Figure IV, D). These modifications correlated well with those of the lateral membrane as they are detectable only in CMs showing high levels of lateral membrane defects. Abnormalities of the ECM structure observed in KO mice most likely related to an impairment of expression of all ECM components/regulators by the CM since their expression levels were all dramatically reduced as measured by quantitative qPCR (Figure 4B). However, the reduced expression of interstitial fibrillar collagens and degradation ECM system by the CM did not impact their expression in the whole cardiac tissue (Online Figure VI). This most probably related to the contribution of the other cardiac cells in the synthesis of the ECM components. In agreement with these observations, we didn't notice any modifications of cardiac collagen I and III levels between WT and KO mice as previously indicated (Online Figure II, A). By contrast, basement membrane components of the CM are specific for the myocyte cell only. Given the importance of the basement membrane in controlling cell morphology, these results suggest that ephrin-B1 maintains lateral membrane morphology of the adult CM by a new mechanism involving regulation of its interaction with the basement membrane. This specific CM-matrix interaction underlies a novel role in the stabilization and organization of the cardiac ECM.

Ephrin-B1 knockdown results in abnormal intercalated disk and sarcomeric structure

Because lateral membrane of the CM is directly connected at both end to the ID which anchors myofilaments, we next examined whether modifications of the lateral membrane in these mice impacted on the different cell-cell junctions of the ID and the sarcomeric apparatus. In opposition to WT mice characterized by ID-components from adherent junction (N-cadherin), desmosomes (desmoplakin 1/2) and gap junctions (connexin-43) regularly organized along the ID (Figure 5A), these proteins demonstrated a significant spatial disorganization of all in the KO mice showing irregular spread dots labelling along a wider ID with no modification of their expression levels (Online Figure VII, A-C). These modifications most likely emanated from ultrastructural alterations of the ID as shown by the higher degree of circumvolution of the ID in electron micrographs from KO hearts (Figure 5B). Beside abnormal ID structure, there was not clear abnormality in the ID space between CMs from WT and KO mice (Online Figure VII, D) nor apparent disorganization in the electron-dense structures associated with the ID or in the myofilaments attachments at these locations. Generally, alteration of proteins directly participating in ID structure influences expression of other ID components [22]. Thus, modification of ID morphology without any modulation of associated-junctional components most likely indicates an indirect consequence of ephrin-B1 deletion linked to the lateral membrane destructuration.

Ephrin-B1 deficient CMs displayed misalignment of both their myofibrils as indicated by rhodamine-phalloïdin staining (Figure 5C) despite no change in the total amount of β-actin (Figure 5D). In correlation with myofibrils structure defects, α-actinin staining also revealed Z-lines misalignment (Figure 5C) associated with significant loss of α-actinin expression (Figure 5D). These changes were detected in all 2 month-old KO mice but still exhibited focal localization within the heart tissue most likely reflecting an indirect consequence of ephrin-B1 deletion at the lateral membrane. Similar Z-lines misalignment was reported in mice models with deletion of intermediate filament (IF) desmin or desmin-associated proteins [23, 24]. However ephrin-B1 KO phenotype is unlikely to be related to desmin deregulation since desmin expression and attachment to Z-lines was preserved (Online Figure VIII, A and B). Finally, despite structural changes in the myofilaments in KO mice, we did not observe any modification of microtubule networks as indicated by similar expression and distribution of tubulin in CMs from WT and KO mice (Online Figure VIII, C and D). Electron microscopy confirmed structural sarcomeric disorganization that could account for disruption of myofibrillar organization (Figure 5E).

Indeed, KO mice exhibited high heterogeneity of their sarcomeres morphology (Online Figure VIII, E-G) together with a lack of actin-enriched I-bands in all sarcomeres (Figure 5E) despite no modification of total actin expression (Figure 5D), most likely indicated relaxed aspect of the sarcomere. Similar ultrastructural abnormalities of sarcomeric apparatus have been observed in the cKO mice (Online Figure IV, E). Again, modification of sarcomeric structure of CMs from KO mice without major modification of its integrity more probably related to indirect consequences of the deletion of ephrin-B1 rather than a direct role of this protein in the contractile apparatus *per se*.

Ephrin-B1 knockdown results in left ventricle chamber dilation and cardiac electrical conduction impairment

To test whether ephrin-B1 played a role in cardiac physiology, we analyzed the cardiac phenotype of *efnb1*$^{-/-}$ mice. At 2 months of age, ephrin-B1 deficient mice (KO, cKO) displayed no difference in heart-to-body weight ratio compared with respective controls (Table 1, upper). Interestingly, echocardiography analysis revealed significant intraventricular dilation in ephrin-B1 KO mice as shown by significant enlargement of the left ventricle at end diastole (LVEDD) with no change in left ventricular wall dimensions (DPWT) or gross alterations in systolic contractile performance compared with WT (Table 1, middle). Enlargement of LVEDD was confirmed in cKO mice but with further significant decrease of IVSTd and DPWT (Table 1, middle). Beside cardiac morphology and contractile function, electric properties of the heart were investigated by electrocardiography. Although depolarization and repolarization of the KO ventricle were normal (QRS complex and QT interval), both *efnb1* KO and cKO mice exhibited significant bradycardia associated with a decrease of the atrioventricular conduction as evidenced by a prolonged PR interval compared with WT mice (Table 1, lower). Taken together, these data indicated that the specific absence of ephrin-B1 in the CM promoted defects in both heart morphology and conduction.

Ephrin-B1 knockdown confers mice hypersensitivity to pressure overload

Given high modifications of cardiac tissue cohesion detected in *efnb1*$^{-/-}$ mice, we assessed its adaptive response to biomechanical stress imposed to the left ventricle under conditions of high blood pressure after ascending aortic banding (AAB) as previously described [25]. Remarkably, 59 % of the ephrin-B1 KO mice died 24 hrs following AAB, compared with no death in the WT group (Figure 6A). While we are uncertain why ephrin-B1 KO mice perished, banded mice that survived developed significant higher hypertrophy response compared with WT after 30 days of AAB as indicated by higher variation of cross-sectional area of myocytes from KO banded (Figure 6 B) and higher variations in interventricular septum (IVST) or LV posterior wall thickness (DPWT) (Online Figure IX, A, Online Table 1 through 3) measured before and after AAB. Interestingly, we measured similar fetal reprogramming and development of reparative fibrosis in KO and WT mice (Online Figure IX, B and C), most likely indicating that the increased hypertrophy detected in KO mice was more related to the morphological defect of the CMs only and not to an increased gene-related compensatory response. This is further supported by the lack of differences in HW/BW ratio between KO and WT mice after AAB. Interestingly, although systolic function was not significantly different 30 days after AAB between WT and KO mice, high EF variability was noticed exclusively in KO, with some animals showing high EF reduction (Figure 6C) correlating with LVEDD dilatation (Figure 6D), thus indicating that ephrin-B1 deletion predisposed to failure. More striking feature of cardiac tissue from KO banded animals came from histomorphologic analysis that revealed fundamental tissue disarray with loss of CM integrity that reminisces that of human patient with end-stage HF (REF Book chapter).Myocytes intersect at various angle and showed whorled appearance, thus indicating a lack of CMs stability within the tissue (Figure 6E, H&E). Modifications in interstitial collagens I and III could not account for the instability of CMs since their gene expression levels were similar in both WT and KO cardiac tissue (Online Figure IX, D). Myofibrils can be seen running in different directions (Figure 6E, H&E, left-middle). Cardiac tissue demonstrated signs of CMs necrosis characterized by cellular swelling, disruption of myofibrils, loss of nuclei and cytoplasmic details and inflammatory cells in close contact to cell debris (Figure 6E, H&E, right). Modifications of CMs were largely evident on WGA-heart sections staining (Figure 6E, WGA). Phenotypic changes of cardiac tissue from KO banded mice also included high dilatation and disorganization of the vessels from the microcirculation which were crossing and interrupting orientation of CMs in the myocardium (Figure

6E, I-B4) despite no change in the capillary network density (Online Figure IX, E). We found high heterogeneity of these features in all KO mice. Interestingly, morphologic cardiac tissue disorganization correlated perfectly with loss of cardiac performance since KO banded mice demonstrating worst shortening fraction exhibited the more dramatic cardiac tissue architecture disarray. In correlation with a putative role of ephrin-B1 in transition toward heart failure, we found that encoding genes for ephrin-B1 and its cognate claudin-5 partner were significantly reduced in CMs from a mouse model of TAC-induced heart failure (Figure 6F) and that ephrin-B1 gene expression positively correlated with EF (Figure 6G). Thus, cardiac expression of ephrin-B1 appears to be crucial for cardioprotective response to severe pressure overload by preserving overall cohesion of cardiac architecture. Altogether, these results highlighted the importance of ephrin-B1 in the adaptative response to pressure overload and suggest its potential role in the transition toward cardiac failure.

Discussion

In this study, we identify ephrin-B1 as a novel component of the lateral membrane of the adult CM. General loss of ephrin-B1 leads to a progressive disorganization of cardiac tissue architecture associated with adult CM morphology defects directly related to the absence of ephrin-B1 at CM the lateral membrane as demonstrated in the conditional cardiomyocyte-specific ephrin-B1 KO mouse model. Ephrin-B1 controls CM morphology through stabilization of the lateral membrane by a novel mechanism most likely involving its interaction with the ECM independently of the mechanotransduction systems. Cardiac architecture abnormalities are associated with an increased left ventricle diameter and delayed atrio-ventricular conduction. Finally, although the absence of ephrin-B1 did not modify compensatory adaptation to pressure overload stress, it precipitates cardiac tissue disorganization classically observed in human HF. These data clearly indicate that ephrin-B1 is an important regulator cardiac tissue architecture that could be involved in cardiac pathologies.

Ephrin-B1 deficiency leads to specific morphological and molecular modification of the lateral membrane of the CM associated with subsequent modifications of the intercalated disk and sarcomeric apparatus structure and loss of ECM integrity. We propose a model whereby ephrin-B1 stabilizes rod-shape adult CM morphology by regulating specific interactions between the lateral membrane and the ECM and thus the tension force distribution at the cell surface (Figure 7). Accordingly, in the absence of ephrin-B1, the CM shrinks and lengthens as a consequence of lateral membrane destabilization thus increasing membrane stiffness as demonstrated by AFM studies. In WT mice, the lateral tension generated by the cell-matrix interaction within the CM could play an indirect role in stretching both sarcomeric apparatus and the ID (Figure 7). To date, only ECM receptors localized all along the sarcolemma of the CM acting were identified as direct lateral tensors for sarcomeres [1, 26-28]. Thus, the lack of ephrin-B1 induces detachment of the lateral membrane from the ECM and as a consequence compresses the ID. As a consequence of ID compaction and because ID structure is known to anchor and stretch myofibrils, CMs exhibit myofibrils misalignment, irregular sarcomere size and loss of visible actin thin strand I-band. Similar modifications have been observed in transgenic mouse models with modifications of ID structure[22]. Finally, misalignment of Z-lines in CMs from *efnb1*$^{-/-}$ mice despite the lack of modification in desmin filaments also most likely related to the loss of lateral tension at the cell membrane. Thus, the decrease of CM width may probably indirectly relax the desmin network attached to the lateral membrane thus mimicking CM features observed in the absence of desmin [23, 24].

Previous studies have already suggested a role for ephrin-B1 in the maintenance of cytomorphology of epithelial cells in the adult kidney [12] as well as for other members from eph/ephrin family in different tissues [13, 14]. However, our data provide first evidence for its importance in stabilization of cardiac tissue architecture independently of cell-cell interaction given the absence of CMs connection through the lateral membrane where it is specifically expressed. Several studies have proposed a role for ephrin-B1 independently of its trans interaction with its cognate Eph receptor [29], for instance by directly interacting in cis with claudin proteins core component of the tight junction. Similarly, ephrin-B1 was found to directly interact with claudin-5 in adult CMs to stabilize its localization at the lateral membrane. Unexpectedly, the presence of claudin-5 in the absence of tight junctions at the lateral membrane suggests a new role for claudin-5. The unusual presence of claudin proteins in non junctional cell membranes was already reported with some isoforms interacting with unrelated transmembrane receptor [30, 31]. However, the functional significance of claudin proteins apart from the intercellular tight junction is currently unknown. Similar observations have already been described for gap junction core components connexins, another class of adhesion molecule, outside the gap junction, where they exhibit new function [32]. The fact that the ephrin-B1/claudin-5 complex was localized all along the plasma membrane could argue for its specific role in directly connecting lateral membrane of the CM to the ECM. However, whether ephrin-B1 or claudin-5 could act as a direct receptor for ECM components has never been shown. Nevertheless, our observations argue for a new role for ephrin-B1 in stabilization of claudin adhesion molecules at the plasma membrane independently of tight junctions.

Ephrin-B1 expression at the lateral membrane of the CM occurs only following the first postnatal days and only during the CM terminal differentiation process (postnatal days 1 to 20) when it acquires its characteristic rod-shape morphology. Because the lateral membrane of the adult CM is required for maintenance of its characteristic rod-like shape, its modification in the ephrin-B1 KO mice could alter the paving shape of the CM as readily observed. Nevertheless, if ephrin-B1 actively participates in the establishment of the lateral membrane and thus the adult CM morphology, one would have expected that in its absence, CMs would never achieve their characteristic rod shape. This is however unlikely since CMs still achieve their mature rod shape in KO mice as evidenced in 3 weeks-old animals and show progressive morphological transformation only after 2 months of age, thus highlighting a role for ephrin-B1 independently of CM maturation initiation process. Therefore, ephrin-B1 more likely plays a role in stabilizing the lateral membrane of the CM subsequently to lateral membrane set up. In line with this assumption, alteration of the adult CMs morphology in the absence of ephrin-B1 appears progressively only after 2 months of age correlating with ephrin-B1 late timing set up at the lateral membrane of the adult CM. Thus, adult CMs morphology defects detected in ephrin-B1 KO mice strikingly referred to the role of ephrin-B1 at the lateral membrane of the mature CM.

Our study highlights a new mechanism involved in CM-ECM interaction specific to the lateral membrane but independent from the classical integrin and dystroglycan systems establishing physical connections between the ECM and the intracellular contractile machinery. Accordingly, mice exhibiting defects in one of these two systems clearly demonstrate specific cardiac contractility defects [33-36]. By opposition and in agreement with integrin or dystroglycan independent pathways, contractile function was preserved in ephrin-B1 KO mice, thus correlating with the lack of dramatic changes in sarcomeric apparatus core components. Moreover, integrity/functionality of the integrin system in ephrin-B1 KO mice is further supported by the expected classical adaptation to pressure overload known to be directly sensed by integrins. Finally, the lack of integrin or dystroglycan components did not lead to structural abnormalities of the lateral membrane as observed in ephrin-B1 KO mice.

Also, it appears that this specific CM lateral membrane-ECM interaction supports a new structural role for the cardiac tissue architecture in maintaining overall integrity of both CMs and the ECM. Similar pattern of ECM disorganization has been already described in hearts from mice lacking collagen XV expression which connects basement membrane of the CM to the fibrillar matrix [37]. The fact that *efnb1*$^{-/-}$ mice exhibited considerable donwregulation of all the components of the basement membrane of the CM most probably arised from a consequence of the disruption of lateral membrane/ECM interaction rather than a direct role on basement membrane synthesis *per se*. In agreement with this hypothesis, 3 weeks old-KO mice show preserved rod-shaped polarized CMs, thus demonstrating the integrity of matrix synthesis at this stage. Similar feedback regulation on laminin synthesis has been already described after disruption of integrin-ECM interaction [38]. Because cellular basement membrane dictates cell morphology, the progressive defects in basement membrane production in ephrin-B1-deficient CMs most probably droved the progressive modification of their rod-shape. The lack of basement membrane components could explain the CMs slippage and thus the tissue architecture disorganization observed following biomechanical stress. Finally, disruption of CM-ECM integrity at the lateral membrane leading to a general lack of cardiac tissue cohesion could account for the increase of the left ventricle diameter measured in KO mice.

One striking feature of *efnb1*$^{-/-}$ mice is their high susceptibility to dazzling death following pressure overload despite higher hypertrophic response, thus suggesting some sort of inadaptation. Although we are not able to determine the exact defect, the observation that KO mice exhibit a delayed atrioventricular conduction together with the morphologic modification of the intercalated disk in CMs with abnormal distribution of connexin 43 could indicate increased arrythmogenic susceptibility in these mice following pressure overload stress. In line with this assumption, recent study showed the importance of heterogeneous connexin 43 distribution in the development of ventricular arrhythmias [39]. The observation that *efnb1*$^{-/-}$ mice exhibit high heterogeneous responses to

pressure overload is also quite intriguing. However, this could be easily explained by the fact that these mice exhibited only focal disorganization of the cardiac tissue at 2 months of age. This is further supported by the histological examination of cardiac tissue from banded KO mice which showed high variations in the degree of cardiac tissue disarray, even if all mice presented these modifications while they were absent in WT mice. Finally, we cannot exclude that disorganization of cardiac vessels detected in KO banded mice is also a contributing factor to death. Further studies using targeted ephrin-B1 deletion will be necessary to explore this hypothesis.

Of interest, our study provided evidence that lack of ephrin-B1 at the CM lateral membrane clearly influences the morphology of the adult CM and its elastic properties. It follows that ephrin-B1 most probably enforces a physical constraint to stabilize the lateral membrane and, in its absence, the CM is more susceptible to external/internal pressures which will directly impact on the CM morphology. This is perfectly illustrated by morphological changes observed in KO and cKO mice exhibiting ventricle dilatation without any modifications of HW/BW, nor reduction in CMs numbers or interstitial ECM. Similarly, this could explain peculiar adaptation of the KO mice during aortic banding with exacerbated increase of CMs area while fetal gene reprogramming and changes in HW/BW are similar to those observed in WT mice.

The exacerbated hypertrophic morphology of the CMs correlating with high tendency to HF in KO banded mice with similar fetal reprogramming and fibrotic compensatory response compared with WT mice, suggests that the intrinsic physical properties of the CM lateral membrane can influence by itself the progression of pathological hypertrophy toward HF independently of the classical hypertrophic reprogramming. In line with this hypothesis, phenotype of banded cardiac tissue from *efnb1*$^{-/-}$ mice reminisces that of human end-stage HF exhibiting high tissue disorganization and loss of CM integrity. Moreover, ephrin-B1 and claudin-5 gene expression were considerably downregulated in CMs from HF mice model. Similar lack of claudin-5 expression was already reported in end-stage HF patients [40]. Finally, EF in mice is directly correlated to the level of ephrin-B1 geen expression.

In summary, we described a previously uncharacterized specific component of the CM lateral membrane, ephrin-B1, which acts as a stabilizer of the CM morphology and the overall cardiac tissue cohesion. Interestingly, ephrin-B1 interacts specifically with claudin-5 which was found to be downregulated in dystrophic mice models or in human end-stage cardiomyopathy [21, 40]. Given our results showing interactions between ephrin-B1 and claudin-5, one might expect similar dysregulation of ephrin-B1 in human cardiomyopathies. In line with this hypothesis, mouse model of DCM associated with claudin-5 downregulation demonstrated similar structural alterations of the lateral membrane as seen in the ephrin-B1 KO mice [21]. Moreover, *efnb1* gene is subjected to large number of mutations in patients with craniofrontonasal syndrome with some patients exhibiting cardiopathy [15]. However, since the role of ephrin-B1 at the adult stage is still new, no study correlating human *efnb1* mutations and the development of cardiomyopathies have been yet performed. To date, HF candidate genes concentrated on proteins involved in regulation/composition of CM contractile apparatus. Our KO model is characterized by an unusual disorganization of the overall cardiac contractile apparatus without classical features observed in models of contractile dysfunction (i.e loss of contractile components, calcium pathway contractile regulators…). Lack of contractile dysfunction in young KO mice suggest the need for future studies in older animal to clarify whether ephrin-B1 is involved in the pathogenesis of cardiomyopathy.

We propose that ephrin-B1, and more generally, structural components of the CM lateral membrane, could directly be involved in occurrence of HF, thus suggesting a novel pathway which needs to be explored beside the classical hypertophic/ fibrotic one.

Acknowledgements

We thank Dr. T. Hébert, J.L. Samuel and B. Swynghedauw for critical reading of the manuscript; Dr R. D'Angelo, JJ Maoret and Childerick Severac for advice and technical assistance regarding imaging (Cellular Imaging Facility IFR150, Rangueil, TRI Platform), qPCR (IFR150-BMT, Quantitative Transcriptomic Platform) and Atomic Force microscopy experiments (Bionanotechnologies platform, Institut des technologies Avancées en sciences du Vivant (ITAV) UMS 3039) respectively.

Sources of funding

This work was supported by BQR grant from Toulouse III Paul Sabatier University (France).

Disclosures

None

References

1. Brancaccio M, Hirsch E, Notte A, Selvetella G, Lembo G, Tarone G. Integrin signalling: the tug-of-war in heart hypertrophy. *Cardiovasc Res.* 2006;70:422-433.
2. Li J, Patel VV, Radice GL. Dysregulation of cell adhesion proteins and cardiac arrhythmogenesis. *Clin Med Res.* 2006;4:42-52.
3. Noorman M, van der Heyden MA, van Veen TA, Cox MG, Hauer RN, de Bakker JM, van Rijen HV. Cardiac cell-cell junctions in health and disease: Electrical versus mechanical coupling. *J Mol Cell Cardiol.* 2009;47:23-31.
4. Lapidos KA, Kakkar R, McNally EM. The dystrophin glycoprotein complex: signaling strength and integrity for the sarcolemma. *Circ Res.* 2004;94:1023-1031.
5. Samarel AM. Costameres, focal adhesions, and cardiomyocyte mechanotransduction. *Am J Physiol Heart Circ Physiol.* 2005;289:H2291-2301.
6. Kullander K, Klein R. Mechanisms and functions of Eph and ephrin signalling. *Nat Rev Mol Cell Biol.* 2002;3:475-486.
7. Kuijper S, Turner CJ, Adams RH. Regulation of angiogenesis by Eph-ephrin interactions. *Trends Cardiovasc Med.* 2007;17:145-151.
8. Pasquale EB. Eph-ephrin bidirectional signaling in physiology and disease. *Cell.* 2008;133:38-52.
9. Merlos-Suarez A, Batlle E. Eph-ephrin signalling in adult tissues and cancer. *Curr Opin Cell Biol.* 2008;20:194-200.
10. Zhao C, Irie N, Takada Y, Shimoda K, Miyamoto T, Nishiwaki T, Suda T, Matsuo K. Bidirectional ephrinB2-EphB4 signaling controls bone homeostasis. *Cell Metab.* 2006;4:111-121.
11. Konstantinova I, Nikolova G, Ohara-Imaizumi M, Meda P, Kucera T, Zarbalis K, Wurst W, Nagamatsu S, Lammert E. EphA-Ephrin-A-mediated beta cell communication regulates insulin secretion from pancreatic islets. *Cell.* 2007;129:359-370.
12. Ogawa K, Wada H, Okada N, Harada I, Nakajima T, Pasquale EB, Tsuyama S. EphB2 and ephrin-B1 expressed in the adult kidney regulate the cytoarchitecture of medullary tubule cells through Rho family GTPases. *J Cell Sci.* 2006;119:559-570.
13. Cooper MA, Son AI, Komlos D, Sun Y, Kleiman NJ, Zhou R. Loss of ephrin-A5 function disrupts lens fiber cell packing and leads to cataract. *Proc Natl Acad Sci U S A.* 2008;105:16620-16625.
14. Stephen LJ, Fawkes AL, Verhoeve A, Lemke G, Brown A. A critical role for the EphA3 receptor tyrosine kinase in heart development. *Dev Biol.* 2007;302:66-79.
15. Twigg SR, Matsumoto K, Kidd AM, Goriely A, Taylor IB, Fisher RB, Hoogeboom AJ, Mathijssen IM, Lourenco MT, Morton JE, Sweeney E, Wilson LC, Brunner HG, Mulliken JB, Wall SA, Wilkie AO. The origin of EFNB1 mutations in craniofrontonasal syndrome: frequent somatic mosaicism and explanation of the paucity of carrier males. *Am J Hum Genet.* 2006;78:999-1010.
16. Davy A, Bush JO, Soriano P. Inhibition of gap junction communication at ectopic Eph/ephrin boundaries underlies craniofrontonasal syndrome. *PLoS Biol.* 2006;4:e315.
17. Lee HS, Nishanian TG, Mood K, Bong YS, Daar IO. EphrinB1 controls cell-cell junctions through the Par polarity complex. *Nat Cell Biol.* 2008;10:979-986.
18. Huynh-Do U, Stein E, Lane AA, Liu H, Cerretti DP, Daniel TO. Surface densities of ephrin-B1 determine EphB1-coupled activation of cell attachment through alphavbeta3 and alpha5beta1 integrins. *Embo J.* 1999;18:2165-2173.

19. Huynh-Do U, Vindis C, Liu H, Cerretti DP, McGrew JT, Enriquez M, Chen J, Daniel TO. Ephrin-B1 transduces signals to activate integrin-mediated migration, attachment and angiogenesis. *J Cell Sci.* 2002;115:3073-3081.
20. Davy A, Aubin J, Soriano P. EphrinB1 forward and reverse signaling are required during mouse development. *Genes Dev.* 2004;18:572-583.
21. Sanford JL, Edwards JD, Mays TA, Gong B, Merriam AP, Rafael-Fortney JA. Claudin-5 localizes to the lateral membranes of cardiomyocytes and is altered in utrophin/dystrophin-deficient cardiomyopathic mice. *J Mol Cell Cardiol.* 2005;38:323-332.
22. Li J, Patel VV, Kostetskii I, Xiong Y, Chu AF, Jacobson JT, Yu C, Morley GE, Molkentin JD, Radice GL. Cardiac-specific loss of N-cadherin leads to alteration in connexins with conduction slowing and arrhythmogenesis. *Circ Res.* 2005;97:474-481.
23. Konieczny P, Fuchs P, Reipert S, Kunz WS, Zeold A, Fischer I, Paulin D, Schroder R, Wiche G. Myofiber integrity depends on desmin network targeting to Z-disks and costameres via distinct plectin isoforms. *J Cell Biol.* 2008;181:667-681.
24. Wang X, Osinska H, Dorn GW, 2nd, Nieman M, Lorenz JN, Gerdes AM, Witt S, Kimball T, Gulick J, Robbins J. Mouse model of desmin-related cardiomyopathy. *Circulation.* 2001;103:2402-2407.
25. Lairez O, Calise D, Bianchi P, Ordener C, Spreux-Varoquaux O, Guilbeau-Frugier C, Escourrou G, Seif I, Roncalli J, Pizzinat N, Galinier M, Parini A, Mialet-Perez J. Genetic deletion of MAO-A promotes serotonin-dependent ventricular hypertrophy by pressure overload. *J Mol Cell Cardiol.* 2009;46:587-595.
26. Danialou G, Comtois AS, Dudley R, Karpati G, Vincent G, Des Rosiers C, Petrof BJ. Dystrophin-deficient cardiomyocytes are abnormally vulnerable to mechanical stress-induced contractile failure and injury. *Faseb J.* 2001;15:1655-1657.
27. Paulin D, Li Z. Desmin: a major intermediate filament protein essential for the structural integrity and function of muscle. *Exp Cell Res.* 2004;301:1-7.
28. Ross RS, Borg TK. Integrins and the myocardium. *Circ Res.* 2001;88:1112-1119.
29. Arvanitis D, Davy A. Eph/ephrin signaling: networks. *Genes Dev.* 2008;22:416-429.
30. Gregory M, Dufresne J, Hermo L, Cyr D. Claudin-1 is not restricted to tight junctions in the rat epididymis. *Endocrinology.* 2001;142:854-863.
31. Harris HJ, Davis C, Mullins JG, Hu K, Goodall M, Farquhar MJ, Mee CJ, McCaffrey K, Young S, Drummer H, Balfe P, McKeating JA. Claudin association with CD81 defines hepatitis C virus entry. *J Biol Chem*;285:21092-21102.
32. Goodenough DA, Paul DL. Beyond the gap: functions of unpaired connexon channels. *Nat Rev Mol Cell Biol.* 2003;4:285-294.
33. Barresi R, Di Blasi C, Negri T, Brugnoni R, Vitali A, Felisari G, Salandi A, Daniel S, Cornelio F, Morandi L, Mora M. Disruption of heart sarcoglycan complex and severe cardiomyopathy caused by beta sarcoglycan mutations. *J Med Genet.* 2000;37:102-107.
34. Milner DJ, Taffet GE, Wang X, Pham T, Tamura T, Hartley C, Gerdes AM, Capetanaki Y. The absence of desmin leads to cardiomyocyte hypertrophy and cardiac dilation with compromised systolic function. *J Mol Cell Cardiol.* 1999;31:2063-2076.
35. Sakamoto A, Ono K, Abe M, Jasmin G, Eki T, Murakami Y, Masaki T, Toyo-oka T, Hanaoka F. Both hypertrophic and dilated cardiomyopathies are caused by mutation of the same gene, delta-sarcoglycan, in hamster: an animal model of disrupted dystrophin-associated glycoprotein complex. *Proc Natl Acad Sci U S A.* 1997;94:13873-13878.

36. Shai SY, Harpf AE, Babbitt CJ, Jordan MC, Fishbein MC, Chen J, Omura M, Leil TA, Becker KD, Jiang M, Smith DJ, Cherry SR, Loftus JC, Ross RS. Cardiac myocyte-specific excision of the beta1 integrin gene results in myocardial fibrosis and cardiac failure. *Circ Res.* 2002;90:458-464.
37. Rasi K, Piuhola J, Czabanka M, Sormunen R, Ilves M, Leskinen H, Rysa J, Kerkela R, Janmey P, Heljasvaara R, Peuhkurinen K, Vuolteenaho O, Ruskoaho H, Vajkoczy P, Pihlajaniemi T, Eklund L. Collagen XV is necessary for modeling of the extracellular matrix and its deficiency predisposes to cardiomyopathy. *Circ Res.* 2010;107:1241-1252.
38. Aumailley M, Pesch M, Tunggal L, Gaill F, Fassler R. Altered synthesis of laminin 1 and absence of basement membrane component deposition in (beta)1 integrin-deficient embryoid bodies. *J Cell Sci.* 2000;113 Pt 2:259-268.
39. Boulaksil M, Winckels SK, Engelen MA, Stein M, van Veen TA, Jansen JA, Linnenbank AC, Bierhuizen MF, Groenewegen WA, van Oosterhout MF, Kirkels JH, de Jonge N, Varro A, Vos MA, de Bakker JM, van Rijen HV. Heterogeneous Connexin43 distribution in heart failure is associated with dispersed conduction and enhanced susceptibility to ventricular arrhythmias. *Eur J Heart Fail*.
40. Mays TA, Binkley PF, Lesinski A, Doshi AA, Quaile MP, Margulies KB, Janssen PM, Rafael-Fortney JA. Claudin-5 levels are reduced in human end-stage cardiomyopathy. *J Mol Cell Cardiol.* 2008;45:81-87.

Table 1. Morphometry and cardiac function of 2 month-old ephrin-B1 WT and KO mice, and of 2 month-old control and c KO mice.

	WT	KO	*control*	c KO
Mice morphometry	***(n=13)***	***(n=18)***	***(n=6)***	***(n=6)***
BW (g)	30.5 ± 4.7	30.0 ± 3.9	25.5 ± 0.2	25.1 ± 0.6
HW (mg)	149 ± 2	152 ± 2	153 ± 4	146 ± 3
HW/BW (mg/g)	4.9 ± 1.0	5.0 ± 0.4	6.0 ± 0.2	5.9 ± 0.2
LW (mg)	188 ± 2	183 ± 2	151 ± 4	143 ± 3
LW/BW (mg/g)	6.2 ± 0.7	6.2 ± 1.2	5.9 ± 0.1	5.7 ± 0.1
Echocardiography	***(n=13)***	***(n=18)***	***(n=6)***	***(n=6)***
IVSTd (mm)	0.83 ± 0.06	0.85 ± 0.07	0.86 ± 0.02	0.80 ± 0,01*
DPWT (mm)	0.86 ± 0.07	0.84 ± 0.08	0.90 ± 0.02	0.80 ± 0,01**
LVEDD (mm)	3.01 ± 0.29	3.41 ± 0,38**	3.17 ± 0.05	3.48 ± 0,05**
LVESD (mm)	2.01 ± 0.25	2.25 ± 0.37	2.13 ± 0.06	2.28 ± 0.07
FS (%)	33.3 ± 3.9	34.4 ± 5.3	33.9 ± 1.2	34.2 ± 1.7
EF (%)	68.7 ± 5.5	69.7 ± 7.1	69.7 ± 1.3	70.0 ± 2.2
Electrocardiography	***(n=20)***	***(n=17)***	***(n=8)***	***(n=9)***
RRi (ms)	172 ± 4	191 ± 6***	132 ± 2	144 ± 3*
PR (ms)	35.4 ± 1.3	39.4 ± 1,1***	37.3 ± 0.5	42.4 ± 1,3*
QRS (ms)	11.7 ± 0.4	11.9 ± 0.8	12.4 ± 1.1	12.8 ± 0.6
QTc (ms)	51.6 ± 3.2	48.5 ± 2.1	51.0 ± 1.7	54.7 ± 2.3

W, body weight; HW, heart weight, LW, lung weight; IVSTd, interventricular septum thickness in diastole; LVEDD, left ventricle end of diastole diameter; DPWT, diastolic posterior wall thickness; LVESD, left ventricle end-systole diameter; FS, fractional shortening; EF, ejection fraction, RRi, RR interval duration; PR, atrio-ventricular conduction time; QRS, complex duration; QTc, duration of QT corrected using Bazett formula.

FIGURE LEGENDS

Figure 1. Localization of ephrin-B1 in the WT mouse heart. (A) Western blot analysis of ephrin-B1 protein levels in cardiac tissue from 2-month old WT mice. Ephrin-B1 cannot be detected in ephrin-B1 KO mice. GAPDH expression was used as reference. **(B)** Immunofluorescence (IF) localization of ephrin-B1 in hearts from 2 month-old WT and KO mice at the plasma membrane of CMs (1), and micro-(2), macrovasculature (3). Specific ephrin-B1 staining is lost in KO mice. **(C)** IF co-localization of ephrin-B1 with CMs lateral membrane and with ECs as shown by Wheat-Germ-Agglutinin (WGA) (**C, upper**) and Isolectin-B4 (I-B4) (**C, lower**) staining respectively in WT mice. Ephrin-B1 is absent from the intercalated disk (**C, upper,** inset). **(D)** Ephrin-B1 immunogold labeling confirmed its localization all along the CM lateral membrane (**left**) and in EC (**right**). bars: 20 μm (**B** and **C**), 5 μm (**C, upper,** inset), 1 μm (**D**).

Figure 2. Progressive cardiac tissue architecture disarray and adult CM morphology alteration in ephrin-B1 KO mice. (**A**) H&E staining of cardiac tissue from 3-week and 2-month old mice showed cardiac tissue disarray in KO mice starting at 2 months of age. (**B**) WGA- IF staining highlighted loss of rod-shape morphology of CMs in KO mice at 2 months of age. (**C**) CMs area from 2-month old mice were measured on WGA-stained heart sections and showed significant decrease of cross-sectional area of CMs from KO mice (n=3-5 per mice lineage group, 50-60 CMs per mouse). (**D**) CMs isolated from 2-month old KO mice displayed a long axis increase and short axis decrease. (n=2 mice per lineage group, 150-180 CMs per mouse). Scale bars: 50 μm (**A** and **B**), 15 μm (**B**, insets), 100 μm (**D**).

Figure 3. Ephrin-B1 stabilizes the lateral membrane structure and stiffness of the CM through a claudin-5 dependant mechanism. (**A**) Electron microscopy shows high disorganization of the lateral membrane in CMs from KO mice. (**B**) (Upper panel) Representative single Indentation curve (plain line) from AFM studies performed on WT (blue, n=3 mice, 4 CMs per mouse, 470 total curves) or KO (red, n=3 mice, 4 CMs per mouse, 528 total curves) living CMs. In both cases, the Hertz model (dotted line) fitted quite well with experiment. (Lower panel) Distribution of the Young Modulus (Elasticity) was homogeneous in WT CMs whereas KO mice exhibited a high standard deviation (larger E distribution). (**C**) Immunofluorescence analysis revealed that ephrin-B1 KO mice lost claudin-5 and ZO-1 proteins localization at the lateral membrane of CMs while delocalizing in the ID and showed (**D**) specific downregulation of claudin-5 protein expression (n=6-7 per mice lineage group) and (**E**) gene expression (n=6 per mice lineage group; ns) as assessed by western-blot and qPCR analysis respectively. (**F**) Ephrin-B1 immunoprecipitation experiments (IP +) followed by western blot analysis on isolated CMs demonstrated the existence of complexes between ephrin-B1, claudin-5 and ZO-1 in WT mice as indicated. Note the lack of ephrin-B1, ZO-1 or claudin-5 immunodetection in KO mice. (IP -), control IP experiments performed in the absence of ephrin-B1 antibody. (**G**) BRET experiments in HEK-293T cells showed specific direct interaction between ephrin-B1 and claudin-5 compared with controls (Soluble GFP2 or α2A transmembrane receptor) (n=3). Scale bars: 1 μm (**A)**, 50 μm **(C),** 25 μm (**C**, insets).

Figure 4. Extracellular matrix defects in ephrin-B1 2-month old KO mice. (**A**) Electron micrographs of interstitial space between lateral membrane of two CMs from WT and KO mice. Note high basement membrane disarray (left, Arrowheads) and fibrillar collagens (right, Arrows) and nonfibrillar protein deposit (asterisks) disorganization in KO mice. (**B**) Comparative qPCR analysis revealed significant decrease of mRNA expression levels of proteins from basement membrane, interstitial ECM (fibrillar collagens), and ECM degradation system (matrix metalloproteinases (MMPs), tissue inhibitors of metalloproteinases (TIMPs)) in total RNA extracts from isolated CMs from KO mice. (n=6-10 per mice lineage group). Scale bars: 0.2 μm (**A).**

Figure 5. Ephrin-B1 KO mice exhibited disorganized intercalated disk (ID) and sarcomeres. (**A**) Immunofluorescence localization of adherent junction (N-cadherin, upper,), desmosomes

(desmoplakin 1/2, middle) and gap junction (connexin 43, lower) in heart sections from 2-month old mice revealed an irregular dot-spot localization of the proteins along the ID in KO mice. (**B**) Distortion of ID ultrastructure could be observed in KO mice (inset highlights simplistic representation of ID morphology). (**C**) Immunofluorescence staining of myofilaments (Rhodamine-phalloidin) or Z-lines (□-actinin) in heart cryosections from 2-month old mice indicated myofibrils and Z-lines misalignment in KO mice correlating (**D**) with downregulation of α-actinin protein expression as shown by Western blot analysis in whole cardiac tissue extracts. No modification of total actin levels was detected (n=6-7 per mice lineage group). (**E**) Ultrastructure of sarcomeres showed loss of I band (WT, arrowheads), misalignment of both myofibrils and sarcomeres in KO mice. Scale bars: 30 µm (**A**), 5 µm (**A**, insets) 0.5 µm (**B**), 10 µm (**C**), 3 µm (**C** inset), 2 µm (**E**), 0.75 µm (**E** inset).

Figure 6. Ephrin-B1 is essential for the cardioprotective response elicited by pressure overload. Two-month old WT or ephrin-B1 KO mice were subjected to ascendant aortic banding (AAB). (**A**) Kaplan-Meier survival analysis of WT (n=27) and KO (n=23) mice. (**B**) CMs area were measured on WGA-stained heart sections and showed significant higher cross-sectional area in KO mice 30 days after AAB (Mean ± SEM, n=6-12 mice per lineage group; *** $P < 0.001$ versus sham control of the same genotype, ## $P < 0.01$, ### $P < 0.001$ versus WT of the same group, unpaired 2-tailed Student's *t* test). (**C**) Echocardiographic measurements of ejection fraction (EF) or (**D**) LVEDD 30 days after AAB showed high hetererogenity in KO mice compared with WT with some mice developing heart failure (Mean and experimental points, n=23 WT, n=18 KO). (**E**) H&E staining of heart sections from WT or KO banded mice identified high disorganization of cardiac tissue architecture in KO mice. Note intersected and whorled CMs (left, middle) as well as CMs necrosis (right, dot-lines, arrowheads). Cell membranes WGA-staining of heart sections confirmed CMs disarray in the myocardium of KO mice. Endothelial cells I-B4 staining of heart sections also identified microcirculation disorganization with some capillaries crossing the myocardium in KO mice (arrowheads). (**F**) Cardiomyocyte *efnb1* and claudin5 gene expression (qPCR) in WT mice submitted to transverse aortic banding (TAC) for 15 days (n=6) or in controls (n=5). (**G**) Linear regression analysis showing the existence of a relationship between CM *efnb1* gene expression level (qPCR) and EF (echocardiography) in WT mice submitted or not to TAC. Scale bars: 100 µm (**E**).

Figure 1

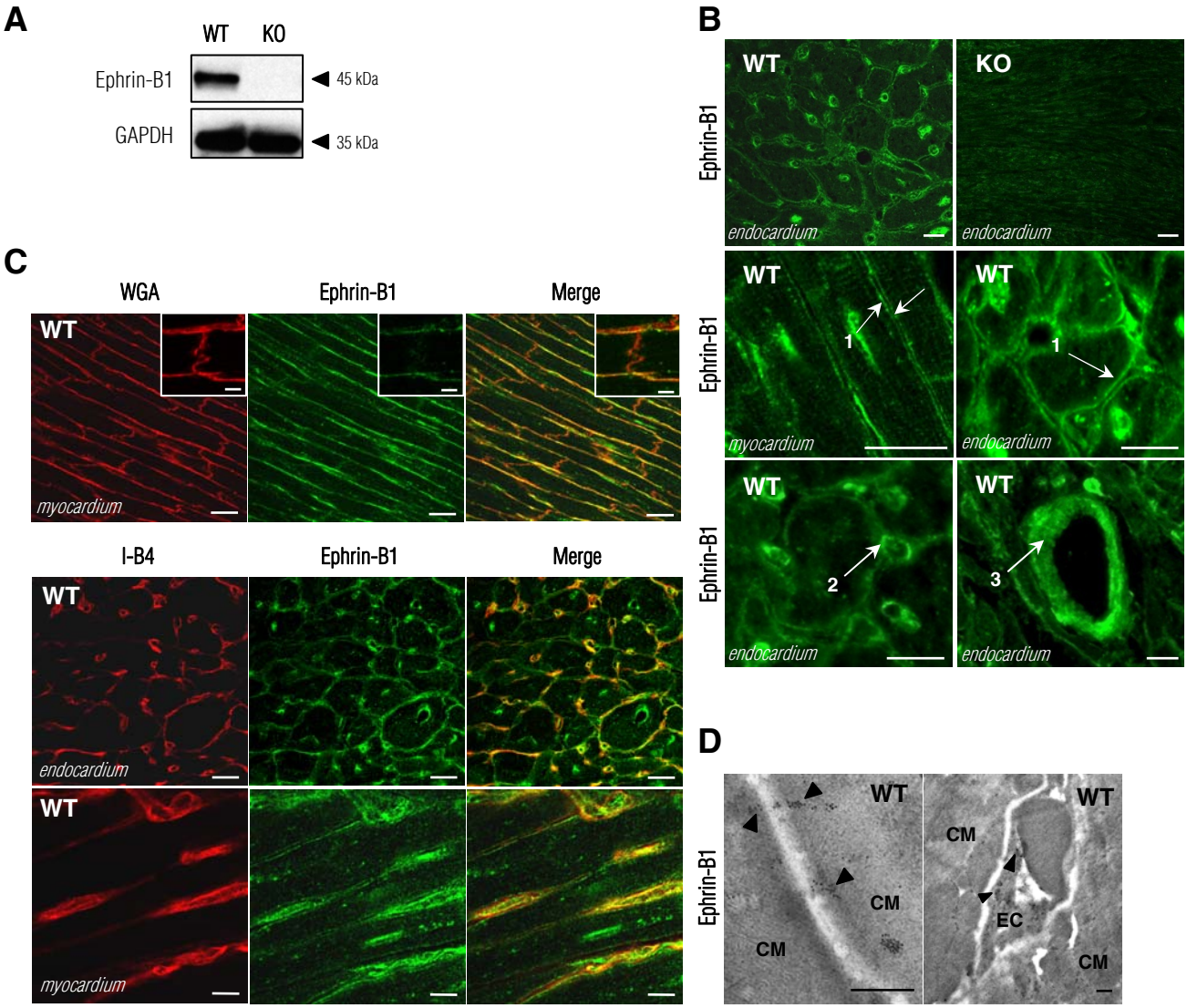

Figure 1. Localization of ephrin-B1 in the WT mouse heart. (A) Western blot analysis of ephrin-B1 protein levels in cardiac tissue from 2-month old WT mice. Ephrin-B1 cannot be detected in ephrin-B1 KO mice. GAPDH expression was used as reference. **(B)** Immunofluorescence (IF) localization of ephrin-B1 in hearts from 2 month-old WT and KO mice at the plasma membrane of CMs (1), and micro-(2), macrovasculature (3). Specific ephrin-B1 staining is lost in KO mice. **(C)** IF co-localization of ephrin-B1 with CMs lateral membrane and with ECs as shown by Wheat-Germ-Agglutinin (WGA) (**C, upper**) and Isolectin-B4 (I-B4) (**C, lower**) staining respectively in WT mice. Ephrin-B1 is absent from the intercalated disk (**C, upper,** inset). **(D)** Ephrin-B1 immunogold labeling confirmed its localization all along the CM lateral membrane (**left**) and in EC (**right**). bars: 20 µm (**B** and **C**), 5 µm (**C, upper,** inset), 1 µm (**D**).

Figure 2

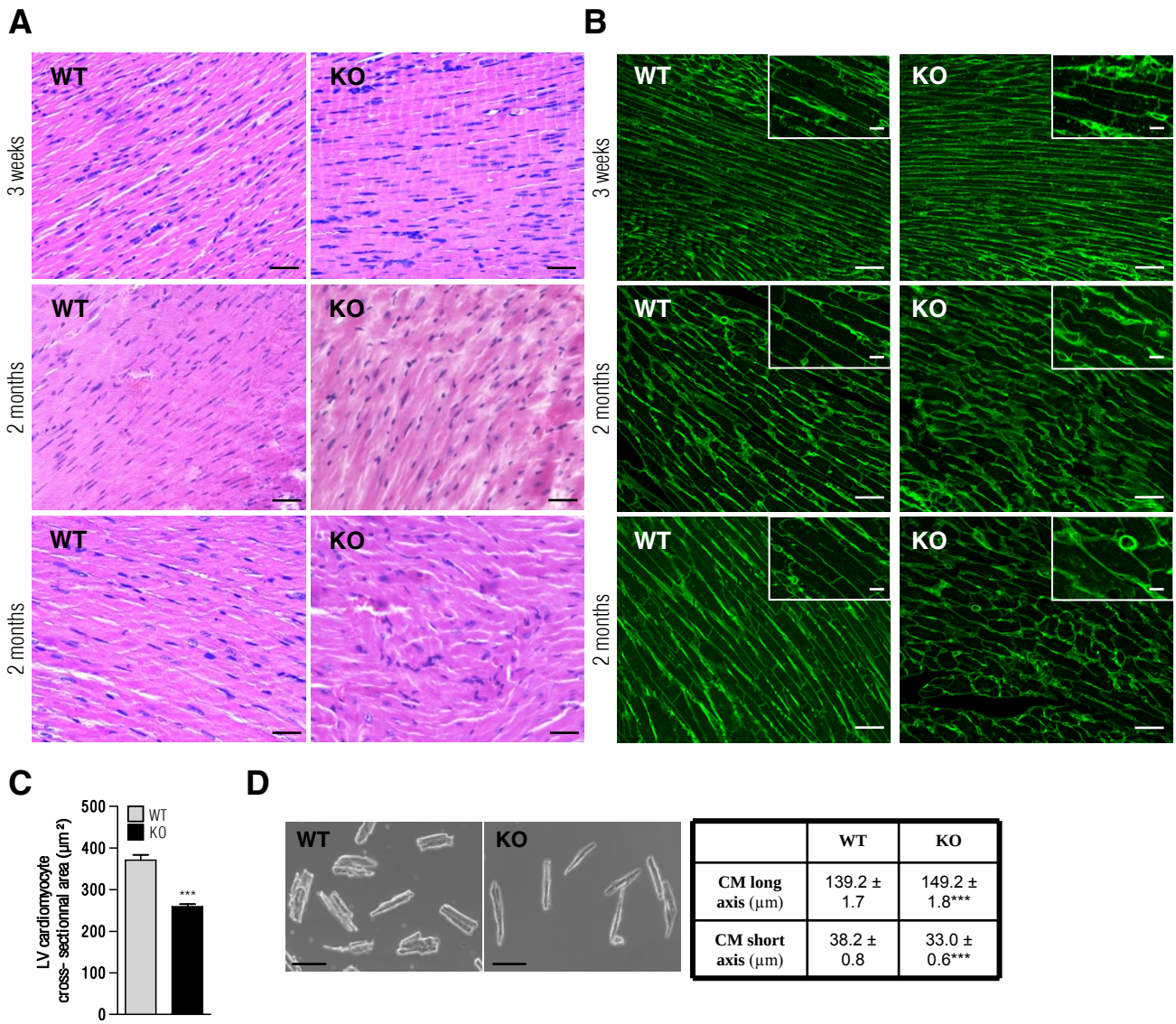

	WT	KO
CM long axis (µm)	139.2 ± 1.7	149.2 ± 1.8***
CM short axis (µm)	38.2 ± 0.8	33.0 ± 0.6***

Figure 2. Progressive cardiac tissue architecture disarray and adult CM morphology alteration in ephrin-B1 KO mice. (**A**) H&E staining of cardiac tissue from 3-week and 2-month old mice showed cardiac tissue disarray in KO mice starting at 2 months of age. (**B**) WGA- IF staining highlighted loss of rod-shape morphology of CMs in KO mice at 2 months of age. (**C**) CMs area from 2-month old mice were measured on WGA-stained heart sections and showed significant decrease of cross-sectional area of CMs from KO mice (n=3-5 per mice lineage group, 50-60 CMs per mouse). (**D**) CMs isolated from 2-month old KO mice displayed a long axis increase and short axis decrease. (n=2 mice per lineage group, 150-180 CMs per mouse). Scale bars: 50 µm (**A** and **B**), 15 µm (**B**, insets), 100 µm (**D**).

Figure 3

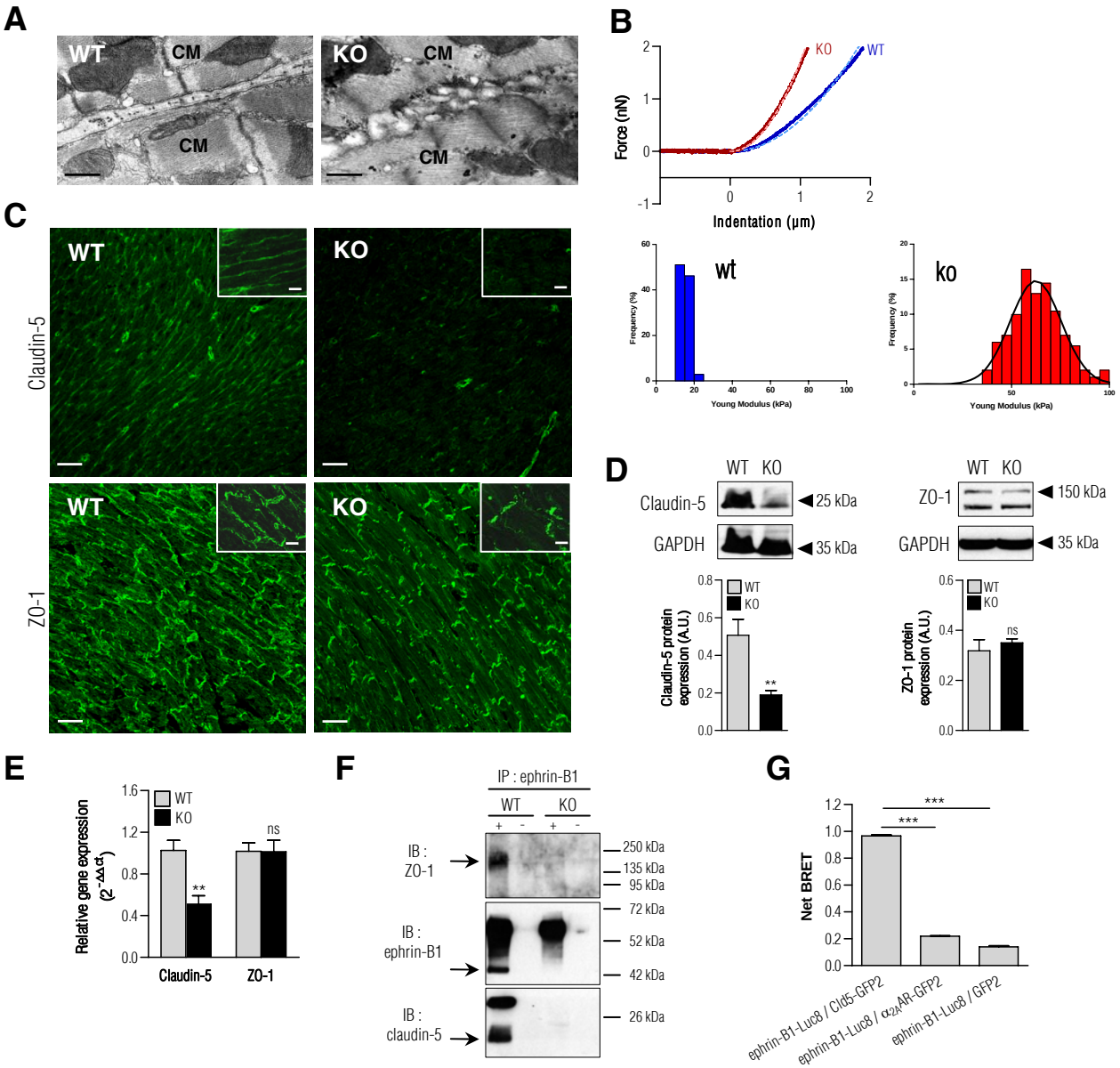

Figure 3. Ephrin-B1 stabilizes the lateral membrane structure and stiffness of the CM through a claudin-5 dependant mechanism. (**A**) Electron microscopy shows high disorganization of the lateral membrane in CMs from KO mice. (**B**) (Upper panel) Representative single Indentation curve (plain line) from AFM studies performed on WT (blue, n=3 mice, 4 CMs per mouse, 470 total curves) or KO (red, n=3 mice, 4 CMs per mouse, 528 total curves) living CMs. In both cases, the Hertz model (dotted line) fitted quite well with experiment. (Lower panel) Distribution of the Young Modulus (Elasticity) was homogeneous in WT CMs whereas KO mice exhibited a high standard deviation (larger E distribution). (**C**) Immunofluorescence analysis revealed that ephrin-B1 KO mice lost claudin-5 and ZO-1 proteins localization at the lateral membrane of CMs while delocalizing in the ID and showed (**D**) specific downregulation of claudin-5 protein expression (n=6-7 per mice lineage group) and (**E**) gene expression (n=6 per mice lineage group; ns) as assessed by western-blot and qPCR analysis respectively. (**F**) Ephrin-B1 immunoprecipitation experiments (IP +) followed by western blot analysis on isolated CMs demonstrated the existence of complexes between ephrin-B1, claudin-5 and ZO-1 in WT mice as indicated. Note the lack of ephrin-B1, ZO-1 or claudin-5 immunodetection in KO mice. (IP -), control IP experiments performed in the absence of ephrin-B1 antibody. (**G**) BRET experiments in HEK-293T cells showed specific direct interaction between ephrin-B1 and claudin-5 compared with controls (Soluble GFP2 or α2A transmembrane receptor) (n=3). Scale bars: 1 µm (**A**), 50 µm **(C),** 25 µm (**C**, insets).

Figure 4

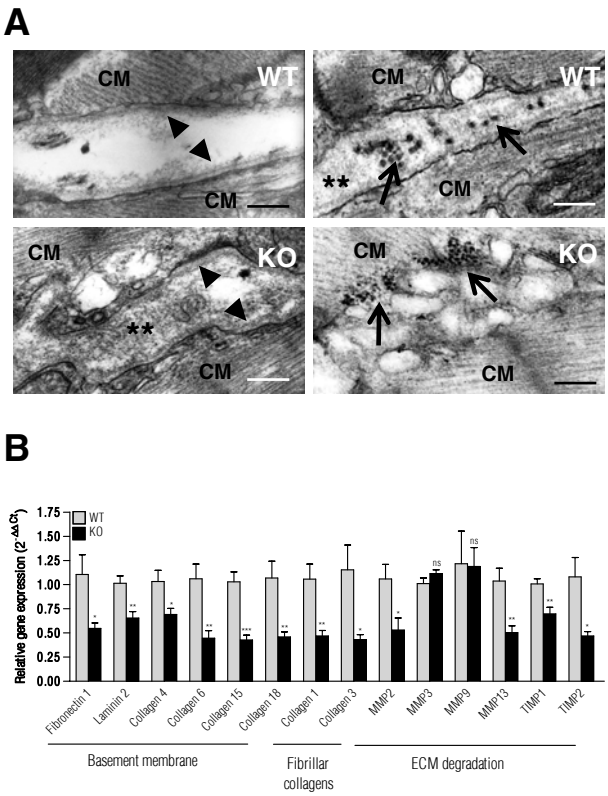

Figure 4. Extracellular matrix defects in ephrin-B1 2-month old KO mice. (**A**) Electron micrographs of interstitial space between lateral membrane of two CMs from WT and KO mice. Note high basement membrane disarray (left, Arrowheads) and fibrillar collagens (right, Arrows) and nonfibrillar protein deposit (asterisks) disorganization in KO mice. (**B**) Comparative qPCR analysis revealed significant decrease of mRNA expression levels of proteins from basement membrane, interstitial ECM (fibrillar collagens), and ECM degradation system (matrix metalloproteinases (MMPs), tissue inhibitors of metalloproteinases (TIMPs)) in total RNA extracts from isolated CMs from KO mice. (n=6-10 per mice lineage group). Scale bars: 0.2 μm (**A).**

Figure 5

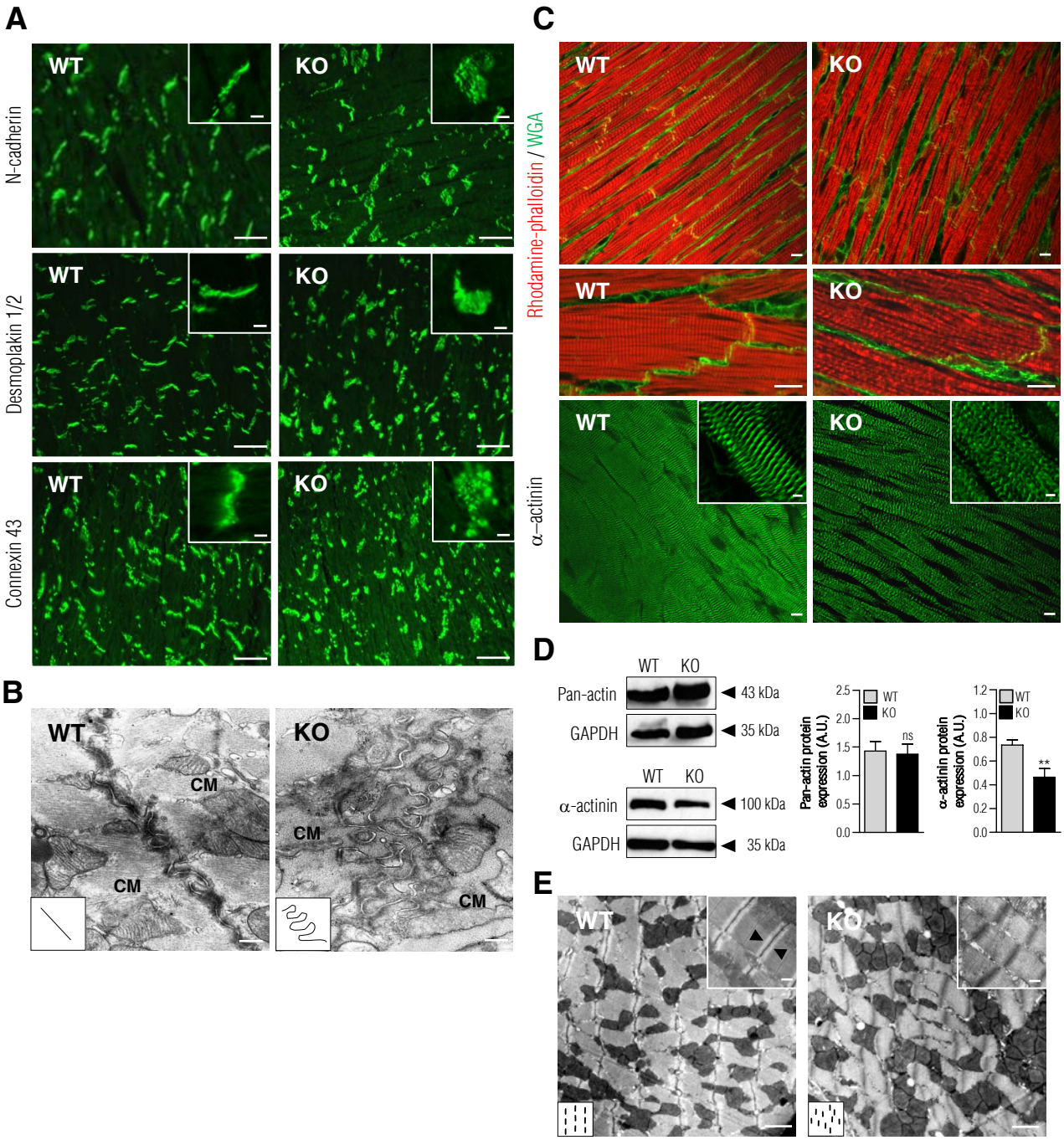

Figure 5. Ephrin-B1 KO mice exhibited disorganized intercalated disk (ID) and sarcomeres. (**A**) Immunofluorescence localization of adherent junction (N-cadherin, upper,), desmosomes (desmoplakin 1/2, middle) and gap junction (connexin 43, lower) in heart sections from 2-month old mice revealed an irregular dot-spot localization of the proteins along the ID in KO mice. (**B**) Distortion of ID ultrastructure could be observed in KO mice (inset highlights simplistic representation of ID morphology). (**C**) Immunofluorescence staining of myofilaments (Rhodamine-phalloidin) or Z-lines (α-actinin) in heart cryosections from 2-month old mice indicated myofibrils and Z-lines misalignment in KO mice correlating (**D**) with downregulation of α-actinin protein expression as shown by Western blot analysis in whole cardiac tissue extracts. No modification of total actin levels was detected (n=6-7 per mice lineage group). (**E**) Ultrastructure of sarcomeres showed loss of I band (WT, arrowheads), misalignment of both myofibrils and sarcomeres in KO mice. Scale bars: 30 µm (**A**), 5 µm (**A**, insets) 0.5 µm (**B**), 10 µm (**C**), 3 µm (**C** inset), 2 µm (**E**), 0.75 µm (**E** inset).

Figure 6

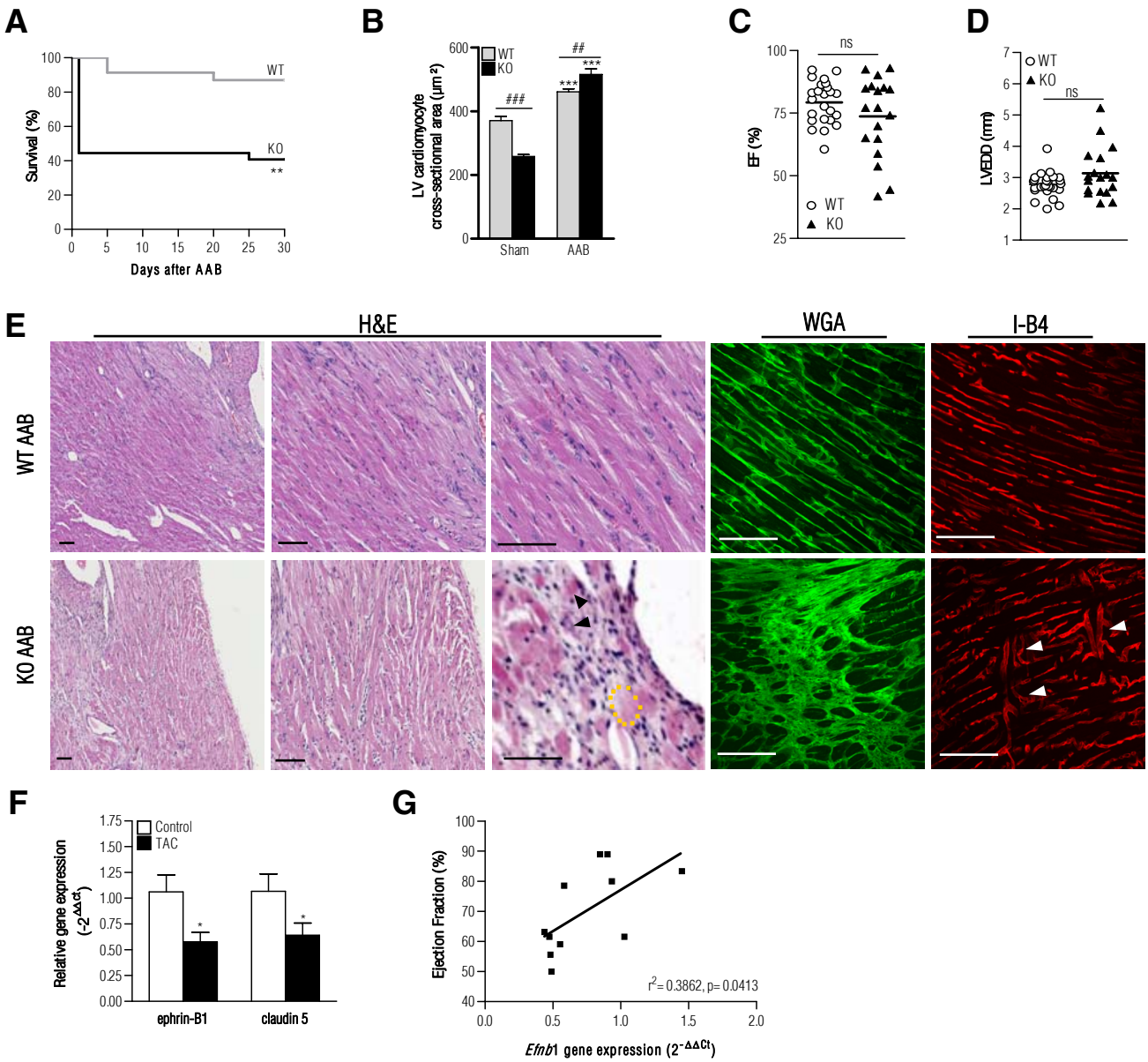

Figure 6. Ephrin-B1 is essential for the cardioprotective response elicited by pressure overload. Two-month old WT or ephrin-B1 KO mice were subjected to ascendant aortic banding (AAB). (**A**) Kaplan-Meier survival analysis of WT (n=27) and KO (n=23) mice. (**B**) CMs area were measured on WGA-stained heart sections and showed significant higher cross-sectional area in KO mice 30 days after AAB (Mean ± SEM, n=6-12 mice per lineage group; *** $P < 0.001$ versus sham control of the same genotype, ## $P < 0.01$, ### $P < 0.001$ versus WT of the same group, unpaired 2-tailed Student's *t* test). (**C**) Echocardiographic measurements of ejection fraction (EF) or (**D**) LVEDD 30 days after AAB showed high hetererogenity in KO mice compared with WT with some mice developing heart failure (Mean and experimental points, n=23 WT, n=18 KO). (**E**) H&E staining of heart sections from WT or KO banded mice identified high disorganization of cardiac tissue architecture in KO mice. Note intersected and whorled CMs (left, middle) as well as CMs necrosis (right, dot-lines, arrowheads). Cell membranes WGA-staining of heart sections confirmed CMs disarray in the myocardium of KO mice. Endothelial cells I-B4 staining of heart sections also identified microcirculation disorganization with some capillaries crossing the myocardium in KO mice (arrowheads). (**F**) Cardiomyocyte *efnb1* and claudin5 gene expression (qPCR) in WT mice submitted to transverse aortic banding (TAC) for 15 days (n=6) or in controls (n=5). (**G**) Linear regression analysis showing the existence of a relationship between CM *efnb1* gene expression level (qPCR) and EF (echocardiography) in WT mice submitted or not to TAC. Scale bars: 100 µm (**E**).

Figure 7

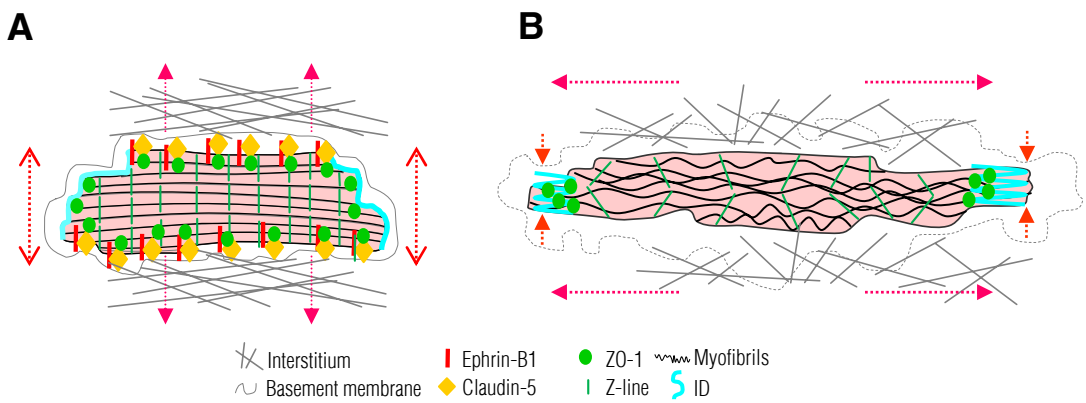

Figure 7. A proposed model for ephrin-B1-mediated stabilization of the adult CM lateral membrane. (**A**) In normal adult CM, ephrin-B1 interacts with claudin-5/ZO-1 complex and stabilizes its localization at the lateral membrane and the interaction of the lateral membrane with the extracellular matrix, thus exerting mechanical tension and stretching both the ID and Z-lines (Red arrows). This interaction maintains ECM structural integrity. (**B**) In the absence of ephrin-B1, claudin-5 disappeared from the lateral membrane while ZO-1 delocalized to the ID and the lateral membrane loses anchorage at the ECM. This leads to morphological modifications of the CM characterized by a long axis increase and short axis decrease (Red arrows) which probably accounts for the increased stiffness of the lateral membrane. Altogether, these lateral membrane alterations indirectly impact on ID, Z-lines, basement membrane and interstitial matrix constitution / organization.

SUPPLEMENTAL MATERIAL

Detailed Methods

Animals. *Efnb1* WT and KO mice were kept in a mixed S129/S4 × C57BL/6 genetic background. As described previously [1], in this background, a fraction of hemizygous null males survive to adulthood. Studies were performed only on males from 3 weeks and 2 months of age. All animal procedures were carried out in accordance with the NIH guidelines and were approved by Midi-Pyrénées animal care and use committee.

Generation of cardiomycoyte-specific ephrin-B1 deficient mice. Mice expressing Cre recombinase driven by the αMHC promoter (pure C57BL/6 genetic background) were crossed with *efnb1*$^{flox/flox}$ mice (pure 129S4 genetic background) to create αMHC-Cre-*efnb1*$^{flox/flox}$ mice (cKO) or littermate control non-Cre-expressing *efnb1*$^{flox/flox}$ mice (control) (mixed C57BL/6×S129/S4 background). Mice carrying a floxed *Efnb1* allele were described previously[1]. Both αMHC-Cre and *efnb1*$^{flox/flox}$ mice were provided by M.D. Schneider (Imperial College London, UK) and A. Davy (Develpment biology center, Toulouse, France) respectively. All experiments using the conditional cardiomyocyte ephrin-B1 KO mice were carried out on males from 2 months of age.

Immunoprecipitation and Western-Blotting. For protein analysis from total cardiac extracts, cardiac tissue samples were directly lysed in RIPA buffer (25 mM Tris-HCl pH 7.6, 150 mM NaCl, 1% NP-40, 1% NaDoc, 0.1% SDS) in the presence of protease inhibitors cocktail (Roche). Immunoprecipitation studies were conducted as previously described [2] from CMs' lysate. Protein concentration of extracts was determined by the Bradford method (Bio-Rad) and equal amounts of proteins were either immunoprecipitated (2 mg) with monoclonal antibody to ephrin-B1 (R&D) or subjected directly (50 μg) to SDS-PAGE and transferred to nitrocellulose membranes (Millipore). Proteins were detected with primary antibodies followed by Horse Radish Peroxydase-conjugated secondary antibodies to goat, mouse, or rabbit IgG (GE Healthcare) using enhanced chemoluminescence detection reagent (GE Healthcare). Proteins quantification was obtained by densitometric analysis using ImageQuant 5.2 software and was normalized to that of GAPDH expression and expressed in arbitraries units (A.U.).

Antibodies. Primary antibodies in this study were : Goat anti-ephrin-B1 (R&D) (It is of note that several commercially available anti-ephrin-B1 antibodies were tested for the ligand detection but only one provided specific staining of the protein as demonstrated by loss of immunodetection in KO mice and this was used for all immunodetection of ephrin-B1); mouse anti-α sarcomeric actinin (Sigma); mouse anti-connexin 43 (Millipore); rabbit anti-N-cadherin (Epitomics); rabbit anti-desmoplakin 1/2 (ARP); mouse anti-β-sarcoglycan (Novacastra); mouse anti-α-dystroglycan (IIH6 clone, Millipore); mouse anti-β1D integrin (Millipore); mouse anti-ZO-1 (Zymed), rabbit anti-claudin 5 (Acris antibodies); goat anti-pan-actin (SantaCruz); rabbit anti-desmin (Cell Signaling Biotechnology); rabbit anti-α tubulin (Epitomics); mouse anti-GAPDH (Abcam). Secondary antibodies, donkey anti-goat OG-488 Alexa Fluor; goat anti-rabbit OG-488-Alexa Fluor, donkey anti-mouse OG-488 Alexa Fluor,

donkey anti-goat Cy3-Alexa Fluor and donkey anti-rat Cy3-Alexa Fluor were all obtained from Invitrogen.
Cell membranes, endothelial cells, nucleus and actin filaments were respectively stained with OG488-conjugated Wheat-Germ-Agglutinin (WGA) (Invitrogen) or OG488-conjugated *Griffonia simplicifolia* isolectin (I-B4) (Invitrogen), TO-PRO-3-iodide (Invitrogen) or tetramethylrhodamine-phalloidine B isothiocyanate (Dako).

Bioluminescence Resonance Energy Transfert (BRET). Plasmid encoding mouse ephrin-B1 was a generous gift from Dr Alice Davy while mouse claudin-5 was cloned from total RNA extracted from mouse lymphatic endothelial SVEC4-10 cell line before subcloning in pcDNA3.1 vector. For $BRET^2$ experiments, ephrin-B1 and claudin-5 were both fused to their C-terminal with *Renillia* Luciferase 8 (Luc8) as energy donor (ephrin-B1-Luc8) or GFP2 as energy acceptor (Cld5-GFP2) respectively. For BRET experiments, HEK293T cells were transiently transfected using PEI method with plasmids encoding ephrin-B1-Luc8 or Cld5-GFP2. Control experiments were performed by transfecting plasmids encoding ephrin-B1-Luc8 together with α_{2A}-AR (α_{2A}-AR-GFP2) [3] as another unrelated transmembrane receptor or soluble GFP2. $BRET^2$ measurements were carried out using comparable total Luc8 luminescence and GFP2 fluorescence in all transfection conditions and performed as previously described [3] using a TECAN INFINITE 500 reader.

Immunohistochemistry and confocal imaging. For histological analysis, hearts were excised and immediately fixed in 10 % formalin, embedded in paraffin and sectioned at 5 µm for hematoxylin-eosin (H&E) staining. Quantification of cardiac interstitial fibrosis was performed from Masson trichrome -stained paraffin-embedded heart sections using Niselement software (Nikon).
For immunofluorescence studies, heart tissue was embedded in OCT and frozen in liquid nitrogen. Frozen sections (5 µm) were fixed with ice-cold acetone followed by permeabilization with 0.1 % Triton X-100 in PBS, blocking (Protein Block, Dako) and incubation with primary antibodies in antibody dilution buffer (0.1 % BSA / 0.1 % Tween 20 / 0.5 % Triton X-100 in PBS). Targeted proteins were visualized with appropriate fluorescence-conjugated secondary antibodies in antibody dilution buffer. Images were acquired with an LSM 510 confocal laser scanning microscope equipped with an Axiovert 200M inverted microscope (Carl Zeiss, Jena, Germany). Zo-1 fluorescence was quantified using Nis-Elements BR2.3 (Nikon) software.
Fluorescent staining of cell membranes (WGA), endothelial cells (I-B4) or actin filaments (phalloidine) were performed on paraffin-embedded heart sections.

Transmission Electron Microscopy (TEM). Heart samples were fixed with 2% glutaraldehyde in Sorensen's buffer. Post-fixation was performed in 1% OsO_4 in Sorensen's buffer for 1 hr followed by dehydratation in ethanol and propylene oxide and embedding in epoxy resin (Epon 812). Ultrathin sections (70 nm) were mounted on 100 mesh collodion-coated copper grids and counterstained with 3% uranyl acetate in 50% ethanol and 8.5% lead citrate before being examined on a HU12A Hitachi electron microscope at 75 KV.

For immunogold staining, tissues were first fixed in 0.1% glutaraldehyde / 2% formaldehyde in 0.1 M phosphate buffer (pH 7.4), washed with 3,5% sucrose and 0.5 M ammonium chloride in 0.1M phosphate buffer. They were finally washed in 0.05 M maleate buffer and prestained with 2% uranyl acetate aqueous solution. Samples were washed with maleate buffer followed by dehydratation in ethanol gradients and then embedded in HM20 resin. After 48 hours of UV-polymerisation, ultrathin sections (70 nm) were mounted on 150 mesh collodion-coated gold grids. Grids were then saturated PBS / 5% BSA and incubated in the presence of anti-ephrin-B1 antibody followed by incubation with secondary gold-labelled anti-goat antibody (10 nm nanogold particles). Grids were finally counterstained with 3% uranyl acetate in 50% ethanol before being examined on a HU12A Hitachi electron microscope at 75 KV.

Cardiomyocytes isolation. For gene expression quantification, ventricular adult CMs were isolated from adult 2 month-old mice using the Langendorff perfusion method as previously described [4]. Briefly, hearts were quickly removed from the chest after euthanasia and the aorta retroperfused with a Ca^{2+}-free bicarbonate-based buffer containing 1mg/ml collagenase (Worthington type II). Following enzymatic digestion, dispersed myocytes were filtered through a 150 μm mesh and gently centrifuged at 500 rpm for 30 seconds. After rinsing, cells were frozen and further used for RNA purification. For Atomic Force Microscopy, immediately after isolation, CMs were plated 20 min on Laminin (Invitrogen) coated plates in CM culture medium (MEM, 5% Fetal Calf Serum, 100 $U.mL^{-1}$ Penicilin, 2 $mM.L^{-1}$ Glutamin) supplemented with 10 mM 2,3-butanedione monoxime (BDM) to inhibit cell contraction.

Measurement of cardiac myocytes surface area and microvascular capillary density. In cardiac tissue, CMs area and capillary density were measured using WGA- or I-B4-stained heart sections respectively. CMs area and capillary density were measured in cross-sectional tissue orientation by manually tracing the cell contour or counting capillaries number respectively on images acquired on Zeiss Observer Z.1 microscope (Carl Zeiss, Jena, Germany) at ×400 (CMs) or ×100 (ECs) magnification and using Axio Vision Rel 4.7 software (Carl Zeiss). For measurements of long and short axis of isolated CMs, cells were plated on Laminin (Invitrogen) coated plates for 15min at 37° C immediately after isolation. Phase-contrast images were acquired on Zeiss Observer Z.1 microscope. Cell size was estimated at the focal plane in which the largest surface was detected. CMs longer and shorter axes were measured using Axio Vision Rel 4.7 software at x100 magnification.

Total RNA isolation and real-time quantitative RT-PCR. Extraction of RNA from cardiac ventricles or isolated adult CMs was performed using Qiagen RNeasy Fibrous Tissue Mini Kit or Qiagen RNeasy Tissue Mini Kit (QIAGEN) respectively. First-strand cDNA was synthesized using the superscript II RT-PCR system (Invitrogen) with random hexamers. Negative controls without reverse transcriptase were made to verify the absence of genomic DNA contamination. Real-time PCR was performed in an ABI 7500 Fast (Applied Biosystems,) in 96-well plates. Twenty-five microliters of cDNA from RT reaction was then mixed with specific primers and EVA green mix (Euromedex). A panel of 5 housekeeping

genes (GAPDH, HPRT, 18S, β2myoglobulin, and PPIA) were tested for their expression stability [5], and geometric mean value of the three housekeeping genes most stably expressed across the samples was used for normalization (GAPDH, HPRT, PPIA). Relative gene expression was calculated by the comparative *Ct* method [6].

Atomic Force Microscopy (AFM). Atomic Force Microscopy experiments were conducted in CM culture medium, at 37 °C under 5% CO_2 flow, using the perfusing cell from the Bioscope Catalyst (Bruker, Santa Barbara, CA, USA). We used bare MLCT AFM probes which present a pyramidal tip, with a curvature radius of 35°, made of Si_3N_4, manufactured by Bruker. The cantilever spring constants were systematically measured using the thermal tune method [7] and has been found to range from 10 to 30 pN/nm. The maximal force applied to the cell has been limited to 2 nN in order to probe the cell wall elasticity (Young Modulus) and not the cell turgor pressure as made at higher loading forces [8, 9] The force (F) *versus* displacement curves were converted into indentation (δ) curves using a homemade software and fitted to the Hertz model [10] (equation 1) taking into account a conical tip with an opening angle of 35° (α). Finally, the Poisson ratio (ν) has been arbitrary fixed to 0.5.

$$F = \frac{2E \tan \alpha}{\pi(1-\nu^2)}\delta^2 \qquad (1)$$

Force curves were recorded on the centre of living cells, on a single point or according to a matrix of 16x16 points on areas of 10 µm². For each force curve the Young Modulus (E) is calculated and the repartition of E plotted on histograms.

Echocardiography. Animals were anesthetized by intraperitoneal injection of 10 µg/g etomidate and underwent noninvasive transthoracic echocardiography using a General Electric Vivid 7® (GE Medical System) equipped with a 14-MHz linear probe. Cardiac ventricular dimensions were measured in M-mode images at least 5 times for each animal. FS was calculated as (LVEDD-LVESD)/LVEDD and expressed as percentage. LV ejection fraction (EF) was calculated using Teichholz formula. Measurements were obtained by an examiner blinded to the genotype of the animals.

Surface ECG recording. A 10 min ECG was obtained under light and 1.5 % isoflurane anaesthesia using three limb leads and digitalized at 4000 Hz. Data were analysed on series of at least 150 consecutive QRS complexes using LabChart Pro (v 6.1.1) software (AD Instruments).

Ascendant Aortic Banding (AAB). Two-month old mice were anesthesized with 4 % isoflurane, ventilated and the left thorax was opened at the second intercostals space. Aortic constriction was performed by legating the ascending aorta using a 7-0 Prolene suture under a dissecting microscope. For this purpose, two nots of a 1.5 mm distance (26-gauge needle circumference), were made on the thread which was carefully introduced around the ascending aorta. Both nots were tight together to perform aortic constriction. Age-matched

animals underwent identical surgical procedure except for ligation of the aorta (sham-operated mice).

Trans Aortic Banding (TAC). Transverse thoracic aortic constriction (TAC) was performed on six-week-old male C57BL/6J mice. Briefly, mice were anesthetized with isofluorane, the chest opened through a small thoracic window and a 27 G needle placed on the transverse aorta. The band was secured using a prolene suture, the needle was then removed and the chest closed. Fifteen days post-surgery, echocardiography was performed and mice were sacrificed for further cardiomyocytes purification and RNA extraction. Both the surgeon and echocardiographer were blinded to animal genotype.

SUPPLEMENTAL FIGURES

SUPPLEMENTAL FIGURES LEGENDS

Online Figure I. Ephrin-B1 expression during postnatal period of the CM. (**A**) Ephrin-B1, Topro-3 (nucleus) and WGA (cell membranes) immunofluorescence co-staining in rat heart cryosections revealed that ephrin-B1 was expressed in CMs at neonatal stage (P0) but only localized in their nuclei (upper panels). Localization of ephrin-B1 at the lateral membrane appeared more lately at the end of the maturation step (P20) (middle, lower panels). (**B**) At neonatal stage, immunofluorescence co-staining revealed that ephrin-B1 was already expressed in endothelial cells (I-B4) (arrow heads). Scale bars: 20 µm (**A** and **B**).

Online Figure II. Histological analysis of cardiac tissue from 2-month old ephrin-B1 WT and KO mice. (**A**) No differences in fibrosis or (**B**) capillary density between 2-month old WT and KO hearts as measured by trichrome or I-B4-stained heart sections respectively. (Mean ± SEM, n=5-7 per mice lineage group, ns, non significant, unpaired 2-tailed Student's *t* test).

Online Figure III. Characterization of α-MHC-Cre$^{+/-}$-*Efnb1*$^{flox/flox}$ mouse (Conditional KO, cKO). (**A**) Exons 2-5 from Ephrin-B1 encoding gene (*efnb1*) are flanked by 2 loxP sites. The primers bind before and after the 3' LoxP. (**B**) A PCR analysis on genomic DNA from tail and isolated cardiomyocytes was performed on 2 month-old α-MHC-Cre$^{+/-}$*efnb1*$^{flox/flox}$ (cKO) and α-MHC-Cre$^{-/-}$*efnb1*$^{flox/flox}$ (Control) mice. **Upper and middle panels** show the □-MHC-Cre and LoxP (*Efnb1* forward primer n°2/*efnb1* reverse primer) amplification into the genome while the **lower panel** shows specific deletion of *efnb1* in ventricular isoled CMs and not from the tail of the same animal as indicated by the detection of the 2 LoxP amplicon in CMs only (*Efnb1* forward primer n°1/*efnb1* reverse primer). (**C**) Western-blot analysis of ephrin-B1 protein expression in isolated CMs from 2-month old control and cKO mice. Ephrin-B1 cannot be detected in CMs from ephrin-B1 cKO mice. (**D**) Immunofluorescence localization of ephrin-B1 in hearts from 2 month-old Control and cKO mice shows a specific deletion of this protein at the lateral membrane of CMs (arrows) from cKO mice while ephrin-B1 expression in endothelial cells (asterisks) is preserved. Scales bars: 20µm (**D**).

Online figure IV. Cardiac characterization of 2 month-old *efnb1* cKO mice. **A**) Electron microscopy shows high disorganization of the lateral membrane in CMs from cKO mice. (**B**) and (**C**) Immunofluorescence analysis revealed that *efnb1* cKO mice lost claudin-5 and ZO-1 proteins localization at the lateral membrane of CMs specifically (arrows). Note that specific claudin-5 expression in endothelial cells (asterisks) is preserved in cKO mice (**D**) Electron micrographs of interstitial space between lateral membrane of two CMs from control and cKO mice. Note high disorganization of fibrillar collagens (arrows) in cKO mice. (**E**) Ultrastructure of sarcomeres show loss of I band (control, arrows), and misalignment of both myofibrils and sarcomeres in cKO mice. Scales bars: 20µm (**A**) 50µm (**B**), 0.75µm (**C** and **E**), 0.2µm (**D**).

Online Figure V. Expression and localization analysis of cell-matrix jonctions of the CMs lateral membrane from 2-month old ephrin-B1 WT and KO mice. (**A**) No modification of localization or (**B**) expression of cell-matrix β1-integrin, β-sarcoglycan and α-dystroglycan proteins in KO mice as assessed by immunofluorescence or Western blot studies respectively (Mean ± SEM, n=4-8 per mice lineage group, ns, non significant, unpaired 2-tailed Student's *t* test). **(C)** Claudin-5 localized specifically at the lateral membrane of CMs from rat hearts as shown by immunofluorescence WGA co-staining. (**D**) ZO-1 localized at

both the lateral membrane and the intercalated disk of isolated CMs as shown by immunofluorescence WGA co-staining. Scale bars: 20 μm (**A** and **C**), 10 μm (**D**).

Online Figure VI. Cell-matrix system expression in total cardiac tissue from 2-month old ephrin-B1 WT and KO mice. Comparative qRT-PCR analysis revealed no difference of mRNA expression levels of proteins from interstitial ECM (fibrillar collagens) and ECM degradation system (matrix metalloproteinases (MMPs), tissue inhibitors of metalloproteinases (TIMPs)) in total RNA cardiac tissue extracts from 2-month old WT and KO mice. (Mean ± SEM, n=6-10 per mice lineage group, ns, non significant, unpaired 2-tailed Student's *t* test).

Online Figure VII. Quantitative analysis of intercalated disk (ID) proteins expression and ID space in 2-month old ephrin-B1 WT and KO mice. No modification of N-cadherin (**A**), desmoplakin 1/2 (**B**) and connexin 43 (**C**) proteins expression between WT and KO mice as assessed by Western blot analysis of whole cardiac tissue extracts (Mean ± SEM, n=4-5 mice per mice lineage group, ns, non significant, unpaired 2-tailed Student's *t* test). (**D**) Measurement of ID space using electron micrographs did not reveal modifications between WT and KO mice. (Mean ± SEM, n=3 mice per lineage group, ns, non significant, unpaired 2-tailed Student's *t* test).

Online Figure VIII. Quantitative analysis of sarcomere associated myofilaments expression and sarcomere ultrastructure in 2-month old ephrin-B1 WT and KO mice. Immunofluorescence staining of desmin (**A**) and α-tubulin (**C**) in heart cryosections and (**B** and **D**) western blot analysis on cardiac extracts from ephrin-B1 WT and KO mice did not reveal modifications of these proteins localization or expression in KO hearts. (Mean ± SEM, n=4 mice per lineage group, ns, non significant, unpaired 2-tailed Student's *t* test). (**E, F, G**) Quantitative analysis of sarcomere ultrastructure in electron micrographs from WT and KO hearts indicated that KO mice showed a significant decrease of sarcomeres length (**E**), increase in sarcomeres width (**F**) and high heterogeneity in Z-lines height (**G**). (Mean ± SEM, n=3 mice per lineage group, 100 independent measurements per mouse; *** $P< 0.001$, unpaired 2-tailed Student's *t* test). Scale bars: 5 μm (**A**), 15 μm (**C**).

Online Figure IX. Histomorphological and genetic profile of cardiac tissue of 2-month old ephrin-B1 WT and KO mice subjected to ascendant aortic banding (AAB). (**A**) IVST (left) and DPWT (right) echocardiographic measurements before and 30 days after AAB showed higher hypertrophic response in KO mice (n=20 WT, n=17 KO). (**B**) WT and KO mice exhibited similar induction of fetal gene program 30 days following AAB (Mean ± SEM, n=7-10 per mice lineage group, ***$P < 0.001$ versus sham control of the same genotype, ns, non significant versus WT of the same group, One-way ANOVA, Tukey test). (**C**) WT and KO mice developed comparable fibrosis as quantified by trichrome-Masson-stained heart sections (Mean ± SEM, n=6-12 mice per lineage group, *$P < 0.05$ versus sham control of the same genotype, ns, non significant versus WT of the same group, unpaired 2-tailed Student's *t* test), in agreement with (**D**) similar induction of fibrotic genes (Mean ± SEM, n=7-10 mice per lineage group, * $P < 0.05$, ***$P < 0.001$ versus sham control of the same genotype, ns, non significant versus WT of the same group, One-way ANOVA, Tukey test). (**E**) Cardiac pressure overload did not modify capillaries density in ephrin-B1 KO mice. Quantification of capillaries density using I-B4 staining heart sections did not reveal modifications between KO and WT mice 30 days after AAB. (Mean ± SEM, n= 6-12 mice per lineage group, ns, non significant versus WT of the same group).

SUPPLEMENTAL TABLES

Online Table 1. Variations of echocardiographic parameters in 2 month-old ephrin-B1 WT and KO mice induced by 30 days aortic ascendant banding (AAB).

	WT *(n=20)*	KO *(n=17)*
IVST (mm)	0.38 ± 0.17	0.53 ± 0.22*
DPWT (mm)	0.34 ± 0.15	0.49 ± 0.28*
LVEDD (mm)	-0.04 ± 0.39	-0.03 ± 0.69
LVESD (mm)	0.37 ± 0.22	0.58 ± 0.21**
FS (%)	4.6 ± 9.8	4.2 ± 15.8
EF (%)	2.7 ± 9.7	1.0 ± 16.3

IVST, Interventricular septum thickness in diastole; DPWT, diastolic posterior wall thickness; LVEDD, left ventricle end-diastole diameter; LVESD, left ventricle end-systole diameter; FS, fractional shortening; EF, ejection fraction. Results are represented as the difference of the parameters measured 30 days after AAB and before AAB. Results are expressed as mean ± SD. *P* values were determined using unpaired 2-tailed Student's *t* test. * $P < 0.05$, ** $P < 0.01$.

Online Table 2. Basal echocardiographic parameters in 2 month-old ephrin-B1 WT and KO mice before aortic ascendant banding.

	WT		KO			
	Sham *(n=7)*	**Banded *(n=27)***	**Sham *(n=6)***	**Banded *(n=18)***	**F**	***P***
IVST (mm)	0.88 ± 0.11	0.91 ± 0.11	0.89 ± 0.06	0.84 ± 0.08	2.12	0.239
DPWT (mm)	0.92 ± 0.13	0.93 ± 0.10	0.97 ± 0.11	0.86 ± 0.08	2.66	0.447
LVEDD (mm)	2.93 ± 0.25	2.87 ± 0.30	3.35 ± 0.33	3.21 ± 0.37°	5.74	0.0019
LVESD (mm)	2.01 ± 0.31	1.77 ± 0.34	1.95 ± 0.42	2.02 ± 0.39	2.11	0.1093
FS (%)	33.7 ± 4.4	37.6 ± 6.4	38.9 ± 4.7	36.7 ± 5.6	1.11	0.3516
EF (%)	69.1 ± 5.3	73.9 ± 7.2	75.8 ± 5.6	72.7 ± 7.4	1.68	0.738
HR (bpm)	524 ± 25	520 ± 57	464 ± 68	462 ± 55°°	4.79	0.0053

IVST, Interventricular septum thickness; DPWT, diastolic posterior wall thickness; LVEDD, left ventricle end-diastole diameter; LVESD, left ventricle end-systole diameter; FS, fractional shortening; EF, ejection fraction; HR, heart rate. Results are expressed as mean ± SD. F values were assessed using one-way ANOVA followed by Bonferroni post-hoc test. ° $P < 0.05$, °° $P < 0.01$ when compared to the corresponding value of the WT lineage group.

Online Table 3. Morphometry and cardiac function of 2 month-old ephrin-B1 WT and KO mice 30 days after aortic ascendant banding.

	WT		KO			
	Sham *(n=7)*	**Banded *(n=27)***	**Sham *(n=6)***	**Banded *(n=18)***	**F**	***P***
IVST (mm)	0.91 ± 0.07	1.29 ± 0.19***	0.90 ± 0.03	1.38 ± 0.21°°°	19.07	<0.0001
DPWT (mm)	0.98 ± 0.11	1.27 ± 0.17**	0.86 ± 0.18	1.35 ± 0.30**	11.16	<0.0001
LVEDD (mm)	2.99 ± 0.23	2.77 ± 0.37	3.42 ± 0.52°	3.26 ± 0.77°	4.24	<0.0094
LVESD (mm)	1.98 ± 0.29	1.66 ± 0.42	2.19 ± 0.53	1.97 ± 0.92	1.75	0.1669
FS (%)	33.7 ± 5.2	42.2 ± 11.9	35.2 ± 4.3	41.0 ± 15.4	1.26	0.2964
EF (%)	69.1 ± 7.2	79.3 ± 8.4	71.0 ± 5.7	73.7 ± 15.9	2.16	0.1040
HR (bpm)	504 ± 47	514 ± 58	449 ± 40°	464 ± 80°	3.00	0.0388
BW (g)	31.7 ± 2.4	30.6 ± 1.8	30.9 ± 2.8	27.5 ± 3.0°	4.46	0.0081
HW (mg)	153 ± 24	183 ± 27	148 ± 25	190 ± 17	3.49	0.0235
HW/BW (mg/g)	5.0 ± 0.9	5.8 ± 0.9	4.8 ± 0.4	6.9 ± 1.9*	6.67	0.0010
LW (mg)	186 ± 22	206 ± 27	187 ± 29	189 ± 34	0.96	0.4220
LW/BW (mg/g)	6.1 ± 0.8	6.5 ± 0.3	6.1 ± 1.0	6.9 ± 1.1	1.06	0.3733

IVST, Interventricular septum thickness; DPWT, diastolic posterior wall thickness; LVEDD, left ventricle end-diastole diameter; LVESD, left ventricle end-systole diameter; FS, fractional shortening; EF, ejection fraction; HR, heart rate; BW, body weight; HW, heart weight; LW, lung weight. Results are expressed as mean ± SD. F values were assessed using one-way ANOVA followed by Bonferroni post-hoc test. * $P < 0.05$, ** $P < 0.01$, *** $P < 0.001$ when compared to the sham value of the same lineage group; ° $P < 0.05$, °°° $P < 0.001$ when compared to the corresponding value of the WT lineage group.

SUPPLEMENTAL REFERENCES

1. Davy A, Aubin J, Soriano P. EphrinB1 forward and reverse signaling are required during mouse development. *Genes Dev.* 2004;18:572-583.
2. Gales C, Kowalski-Chauvel A, Dufour MN, Seva C, Moroder L, Pradayrol L, Vaysse N, Fourmy D, Silvente-Poirot S. Mutation of Asn-391 within the conserved NPXXY motif of the cholecystokinin B receptor abolishes Gq protein activation without affecting its association with the receptor. *J Biol Chem.* 2000;275:17321-17327.
3. Gales C, Van Durm JJ, Schaak S, Pontier S, Percherancier Y, Audet M, Paris H, Bouvier M. Probing the activation-promoted structural rearrangements in preassembled receptor-G protein complexes. *Nat Struct Mol Biol.* 2006;13:778-786.
4. Hilal-Dandan R, Kanter JR, Brunton LL. Characterization of G-protein signaling in ventricular myocytes from the adult mouse heart: differences from the rat. *J Mol Cell Cardiol.* 2000;32:1211-1221.
5. Vandesompele J, De Preter K, Pattyn F, Poppe B, Van Roy N, De Paepe A, Speleman F. Accurate normalization of real-time quantitative RT-PCR data by geometric averaging of multiple internal control genes. *Genome Biol.* 2002;3:RESEARCH0034.
6. Livak KJ, Schmittgen TD. Analysis of relative gene expression data using real-time quantitative PCR and the 2(-Delta Delta C(T)) Method. *Methods.* 2001;25:402-408.
7. Emerson RJt, Camesano TA. On the importance of precise calibration techniques for an atomic force microscope. *Ultramicroscopy.* 2006;106:413-422.
8. Arnoldi M, Fritz M, Bauerlein E, Radmacher M, Sackmann E, Boulbitch A. Bacterial turgor pressure can be measured by atomic force microscopy. *Phys Rev E Stat Phys Plasmas Fluids Relat Interdiscip Topics.* 2000;62:1034-1044.
9. Yao X, Walter J, Burke S, Stewart M, MH J, Pink D, Hunter R, Beveridge T. Atomic force microscopy and theorithical considerations of surface properties and turgor pressures of bacteria. *Colloids and Surfaces B: Biointerfaces.* 2002;23:213-230.
10. Hertz H. Ueber die Berünhrung fester elastischer Körper. *Journal für die Reine und angewandte mathematik.* 1881;92:156-171.

Online Figure I

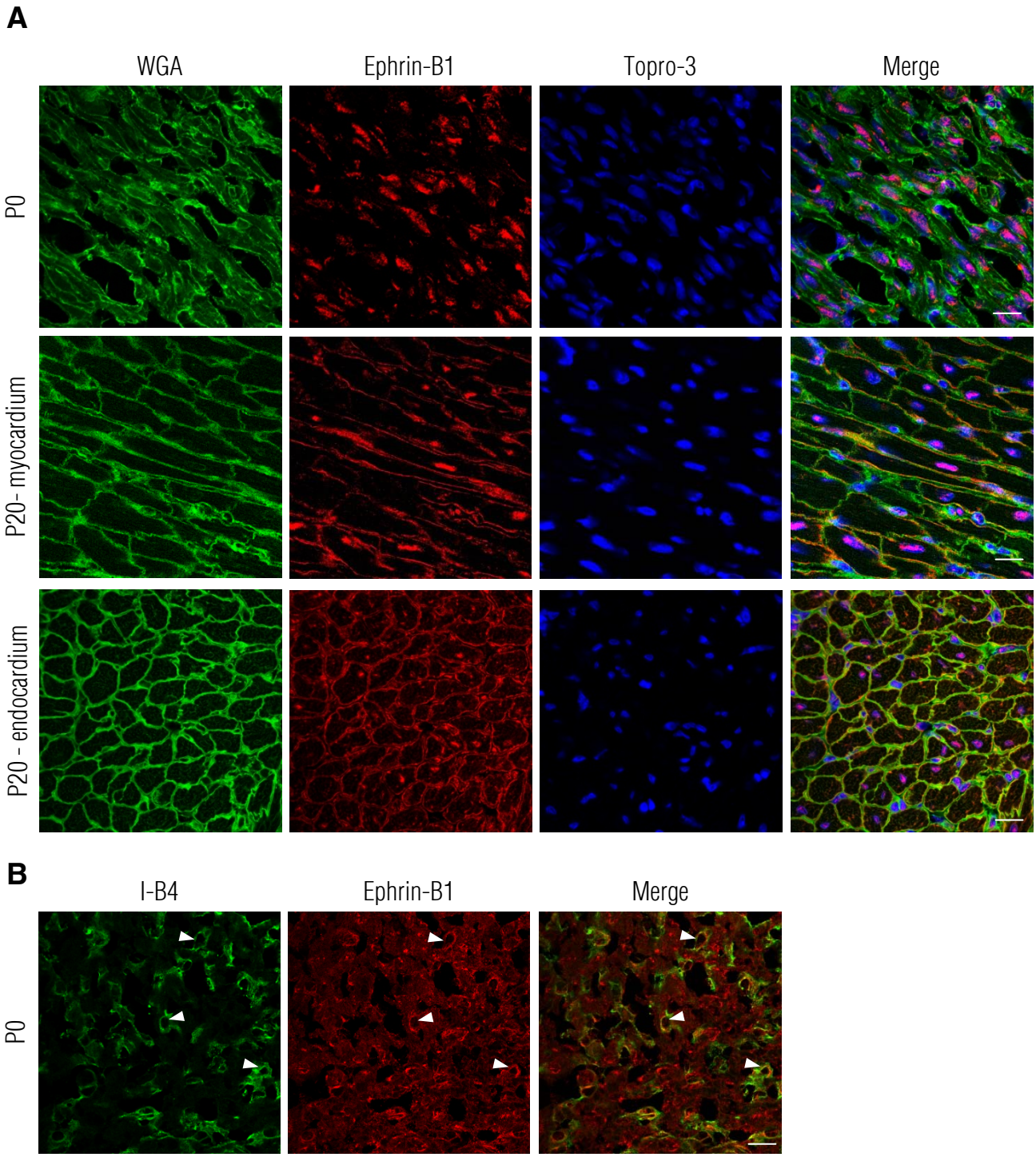

Online Figure I. Ephrin-B1 expression during postnatal period of the CM. (**A**) Ephrin-B1, Topro-3 (nucleus) and WGA (cell membranes) immunofluorescence co-staining in rat heart cryosections revealed that ephrin-B1 was expressed in CMs at neonatal stage (P0) but only localized in their nuclei (upper panels). Localization of ephrin-B1 at the lateral membrane appeared more lately at the end of the maturation step (P20) (middle, lower panels). (**B**) At neonatal stage, immunofluorescence co-staining revealed that ephrin-B1 was already expressed in endothelial cells (I-B4) (arrow heads). Scale bars: 20 µm (**A** and **B**).

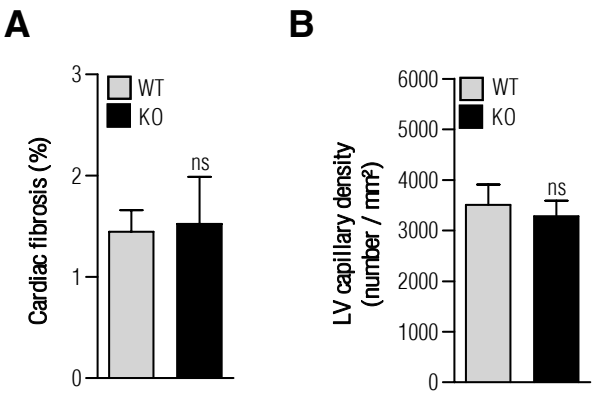

Online Figure II. Histological analysis of cardiac tissue from 2-month old ephrin-B1 WT and KO mice. (**A**) No differences in fibrosis or (**B**) capillary density between 2-month old WT and KO hearts as measured by trichrome or I-B4-stained heart sections respectively. (Mean ± SEM, n=5-7 per mice lineage group, ns, non significant, unpaired 2-tailed Student's *t* test).

Online Figure III

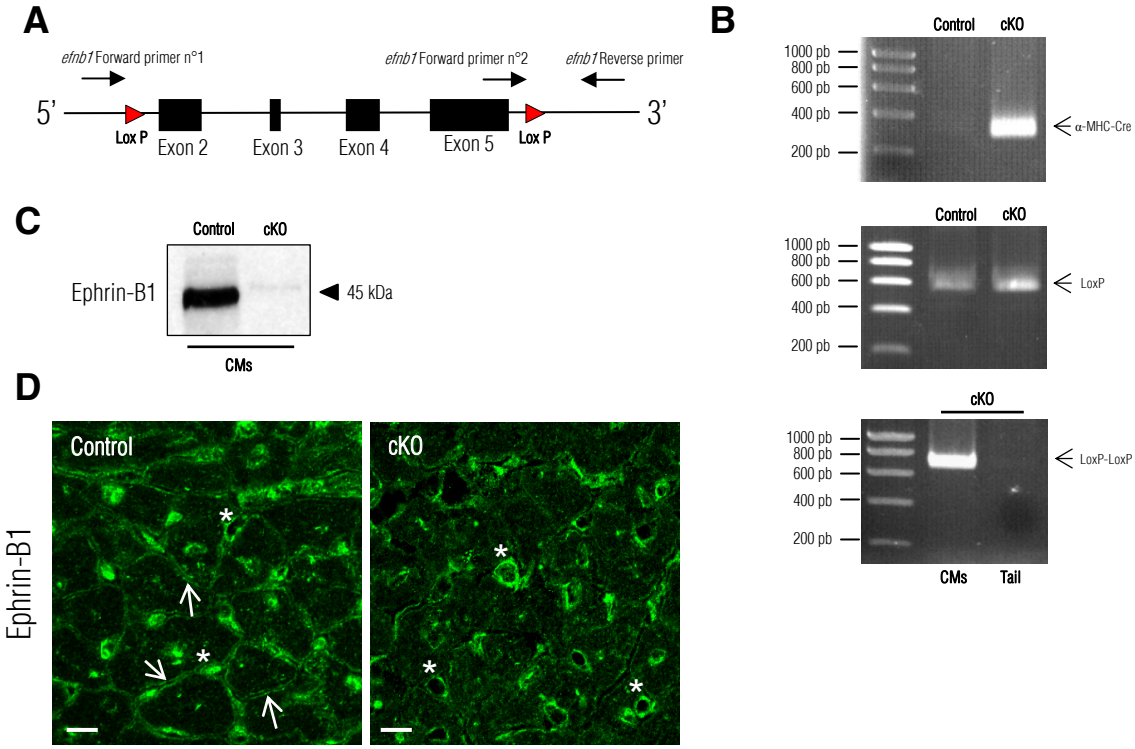

Online Figure III. Characterization of α-MHC-Cre$^{+/-}$-*Efnb1*$^{flox/flox}$ mouse (Conditional KO, cKO). (**A**) Exons 2-5 from Ephrin-B1 encoding gene (*efnb1*) are flanked by 2 loxP sites. The primers bind before and after the 3' LoxP. (**B**) A PCR analysis on genomic DNA from tail and isolated cardiomyocytes was performed on 2 month-old α-MHC-Cre$^{+/-}$*efnb1*$^{flox/flox}$ (cKO) and α-MHC-Cre$^{-/-}$*efnb1*$^{flox/flox}$ (Control) mice. **Upper and middle panels** show the α-MHC-Cre and LoxP (*Efnb1* forward primer n°2/*efnb1* reverse primer) amplification into the genome while the **lower panel** shows specific deletion of *efnb1* in ventricular isoled CMs and not from the tail of the same animal as indicated by the detection of the 2 LoxP amplicon in CMs only (*Efnb1* forward primer n°1/*efnb1* reverse primer). (**C**) Western-blot analysis of ephrin-B1 protein expression in isolated CMs from 2-month old control and cKO mice. Ephrin-B1 cannot be detected in CMs from ephrin-B1 cKO mice. (**D**) Immunofluorescence localization of ephrin-B1 in hearts from 2 month-old Control and cKO mice shows a specific deletion of this protein at the lateral membrane of CMs (arrows) from cKO mice while ephrin-B1 expression in endothelial cells (asterisks) is preserved. Scales bars: 20µm (**D**).

Online Figure IV

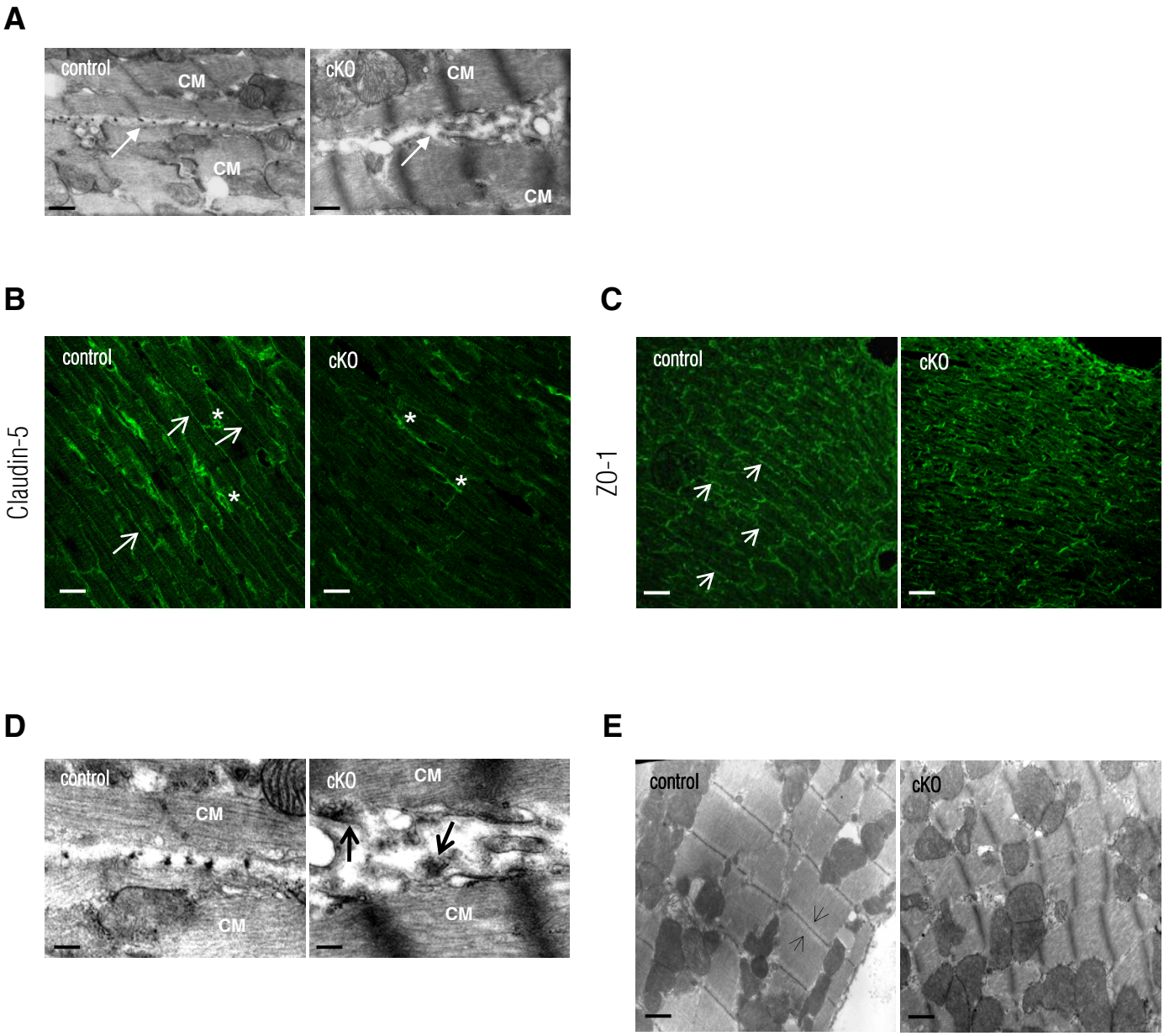

Online figure IV. Cardiac characterization of 2 month-old *efnb1* cKO mice. **A**) Electron microscopy shows high disorganization of the lateral membrane in CMs from cKO mice. (**B**) and (**C**) Immunofluorescence analysis revealed that *efnb1* cKO mice lost claudin-5 and ZO-1 proteins localization at the lateral membrane of CMs specifically (arrows). Note that specific claudin-5 expression in endothelial cells (asterisks) is preserved in cKO mice (**D**) Electron micrographs of interstitial space between lateral membrane of two CMs from control and cKO mice. Note high disorganization of fibrillar collagens (arrows) in cKO mice. (**E**) Ultrastructure of sarcomeres show loss of I band (control, arrows), and misalignment of both myofibrils and sarcomeres in cKO mice. Scales bars: 20µm (**A**) 50µm (**B**), 0.75µm (**C** and **E**), 0.2µm (**D**).

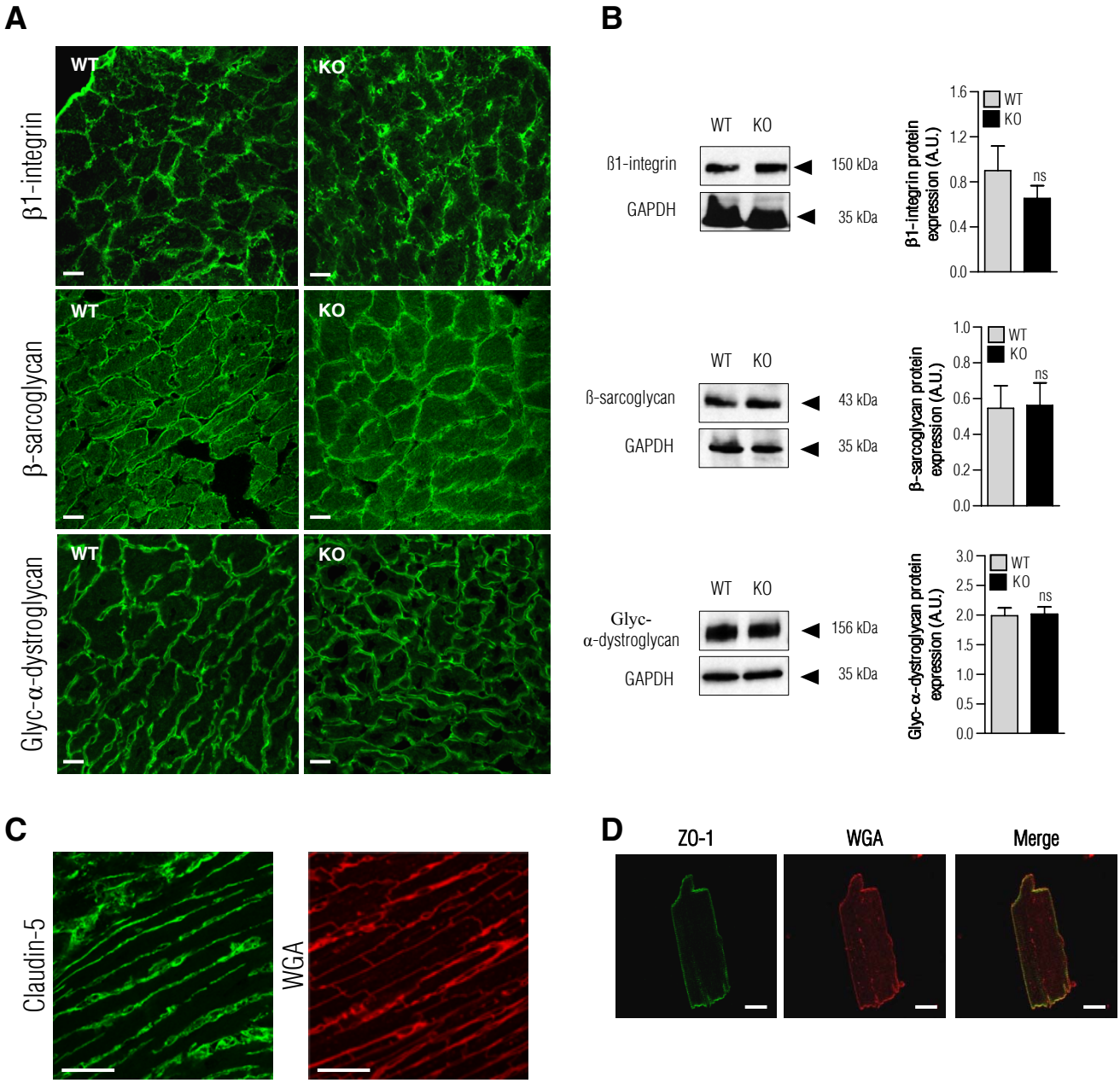

Online Figure V. Expression and localization analysis of cell-matrix jonctions of the CMs lateral membrane from 2-month old ephrin-B1 WT and KO mice. (**A**) No modification of localization or (**B**) expression of cell-matrix β1-integrin, β-sarcoglycan and α-dystroglycan proteins in KO mice as assessed by immunofluorescence or Western blot studies respectively (Mean ± SEM, n=4-8 per mice lineage group, ns, non significant, unpaired 2-tailed Student's *t* test). **(C)** Claudin-5 localized specifically at the lateral membrane of CMs from rat hearts as shown by immunofluorescence WGA co-staining. (**D**) ZO-1 localized at both the lateral membrane and the intercalated disk of isolated CMs as shown by immunofluorescence WGA co-staining. Scale bars: 20 µm (**A** and **C**), 10 µm (**D**).

Online Figure VI

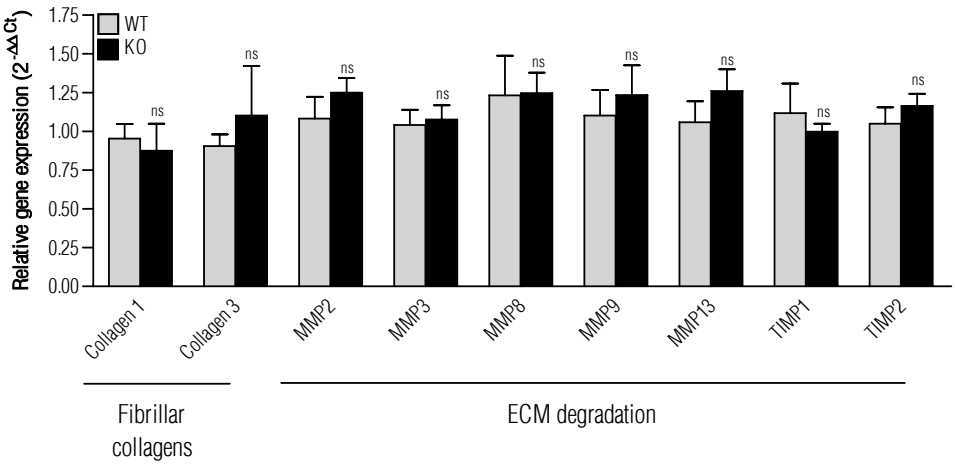

Online Figure VI. Cell-matrix system expression in total cardiac tissue from 2-month old ephrin-B1 WT and KO mice. Comparative qRT-PCR analysis revealed no difference of mRNA expression levels of proteins from interstitial ECM (fibrillar collagens) and ECM degradation system (matrix metalloproteinases (MMPs), tissue inhibitors of metalloproteinases (TIMPs)) in total RNA cardiac tissue extracts from 2-month old WT and KO mice. (Mean ± SEM, n=6-10 per mice lineage group, ns, non significant, unpaired 2-tailed Student's *t* test).

Online Figure VII

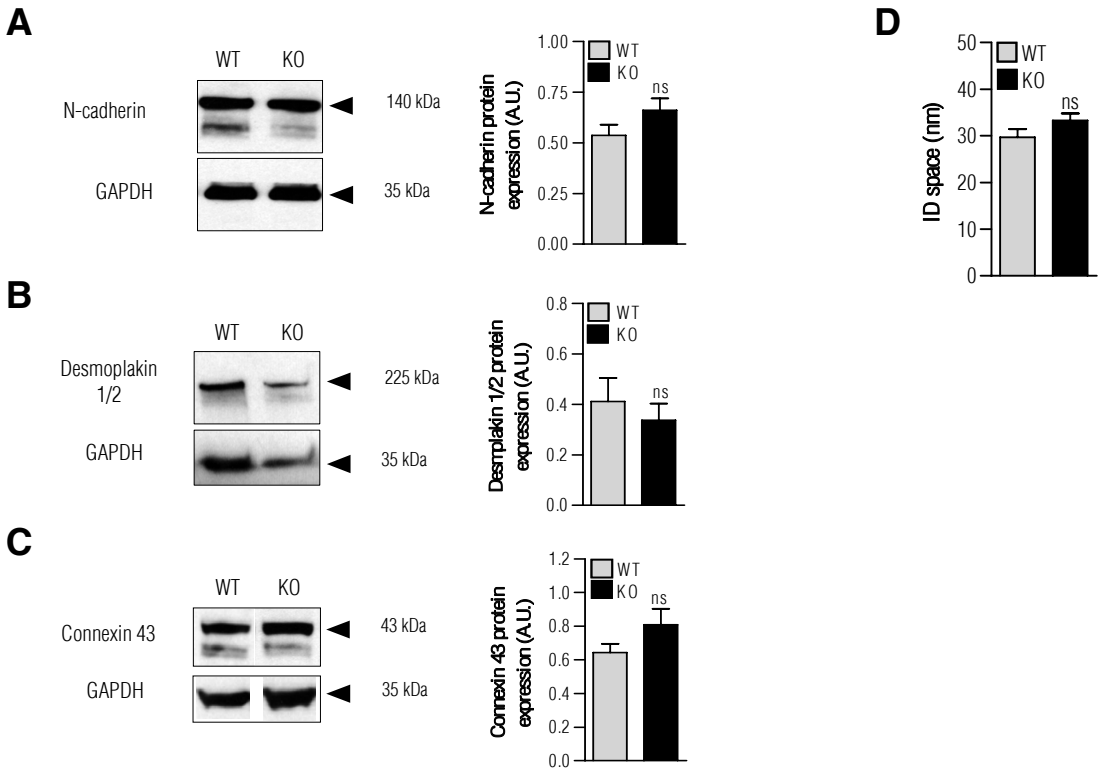

Online Figure VII. Quantitative analysis of intercalated disk (ID) proteins expression and ID space in 2-month old ephrin-B1 WT and KO mice. No modification of N-cadherin (**A**), desmoplakin 1/2 (**B**) and connexin 43 (**C**) proteins expression between WT and KO mice as assessed by Western blot analysis of whole cardiac tissue extracts (Mean ± SEM, n=4-5 mice per mice lineage group, ns, non significant, unpaired 2-tailed Student's *t* test). (**D**) Measurement of ID space using electron micrographs did not reveal modifications between WT and KO mice. (Mean ± SEM, n=3 mice per lineage group, ns, non significant, unpaired 2-tailed Student's *t* test).

Online Figure VIII

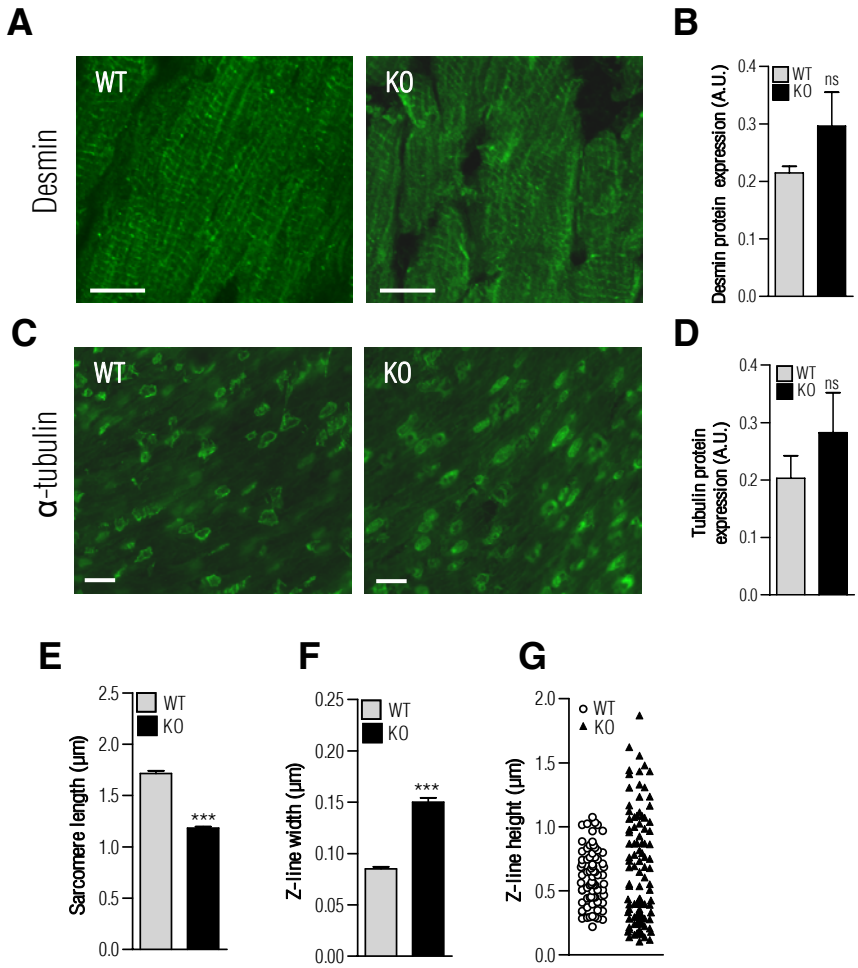

Online Figure VIII. Quantitative analysis of sarcomere associated myofilaments expression and sarcomere ultrastructure in 2-month old ephrin-B1 WT and KO mice. Immunofluorescence staining of desmin (**A**) and α-tubulin (**C**) in heart cryosections and (**B** and **D**) western blot analysis on cardiac extracts from ephrin-B1 WT and KO mice did not reveal modifications of these proteins localization or expression in KO hearts. (Mean ± SEM, n=4 mice per lineage group, ns, non significant, unpaired 2-tailed Student's *t* test). (**E, F, G**) Quantitative analysis of sarcomere ultrastructure in electron micrographs from WT and KO hearts indicated that KO mice showed a significant decrease of sarcomeres length (**E**), increase in sarcomeres width (**F**) and high heterogeneity in Z-lines height (**G**). (Mean ± SEM, n=3 mice per lineage group, 100 independent measurements per mouse; *** $P< 0.001$, unpaired 2-tailed Student's *t* test). Scale bars: 5 µm (**A**), 15 µm (**C**).

Online Figure IX

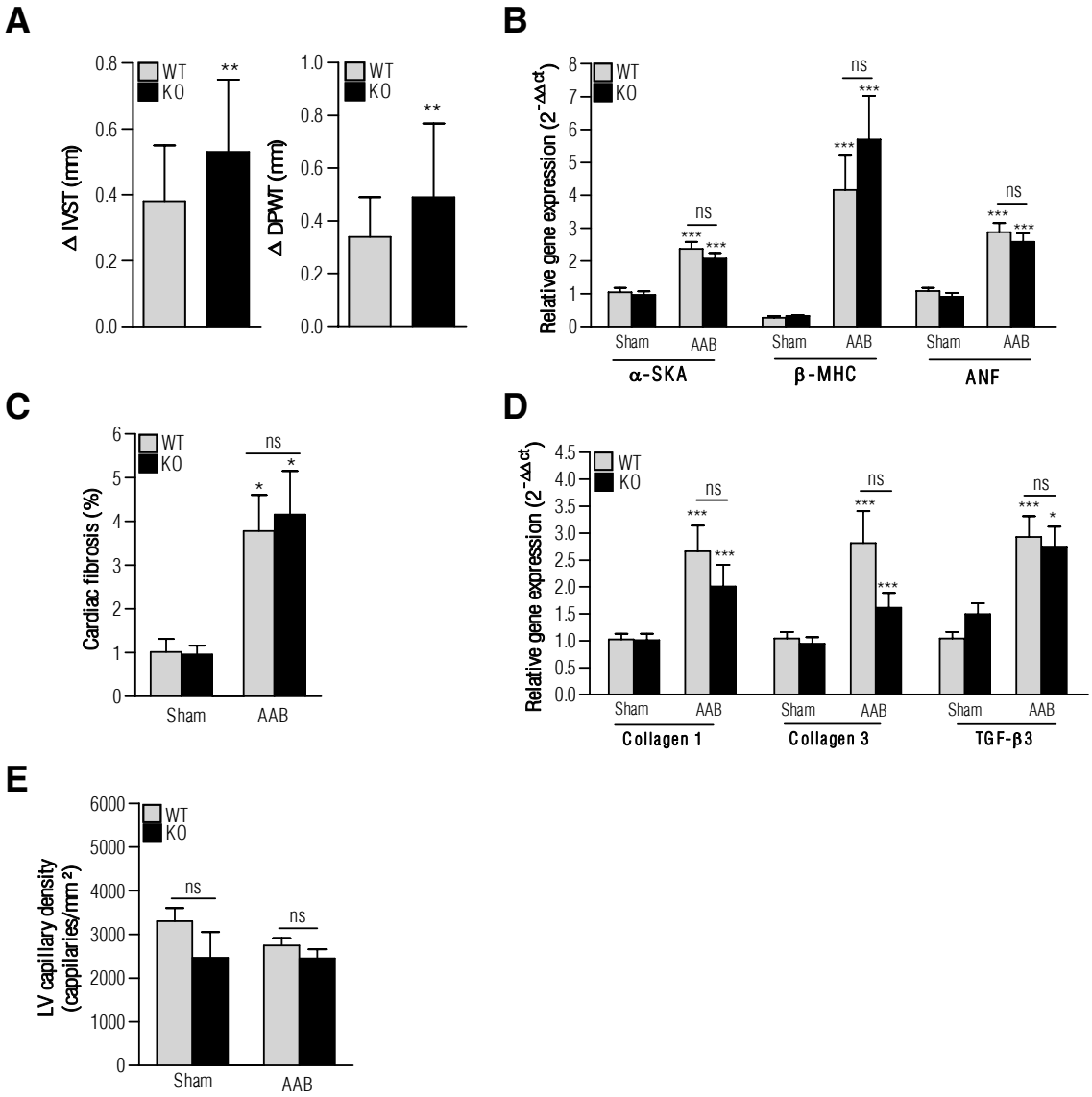

Online Figure IX. Histomorphological and genetic profile of cardiac tissue of 2-month old ephrin-B1 WT and KO mice subjected to ascendant aortic banding (AAB). (**A**) IVST (left) and DPWT (right) echocardiographic measurements before and 30 days after AAB showed higher hypertrophic response in KO mice (n=20 WT, n=17 KO). (**B**) WT and KO mice exhibited similar induction of fetal gene program 30 days following AAB (Mean ± SEM, n=7-10 per mice lineage group, ***$P < 0.001$ versus sham control of the same genotype, ns, non significant versus WT of the same group, One-way ANOVA, Tukey test). (**C**) WT and KO mice developed comparable fibrosis as quantified by trichrome-Masson-stained heart sections (Mean ± SEM, n=6-12 mice per lineage group, *$P < 0.05$ versus sham control of the same genotype, ns, non significant versus WT of the same group, unpaired 2-tailed Student's *t* test), in agreement with (**D**) similar induction of fibrotic genes (Mean ± SEM, n=7-10 mice per lineage group, * $P < 0.05$, ***$P < 0.001$ versus sham control of the same genotype, ns, non significant versus WT of the same group, One-way ANOVA, Tukey test). (**E**) Cardiac pressure overload did not modify capillaries density in ephrin-B1 KO mice. Quantification of capillaries density using I-B4 staining heart sections did not reveal modifications between KO and WT mice 30 days after AAB. (Mean ± SEM, n= 6-12 mice per lineage group, ns, non significant versus WT of the same group).